การศึกษาการทำงานของระบบปรับปริมาณรังสีอัตโนมัติของเครื่องเอกซเรย์คอมพิวเตอร์ด้วยหุ่นจำลอง

นางสาวสุพรรณี ภาสองชั้น

วิทยานิพนธ์นี้เป็นส่วนหนึ่งของการศึกษาตามหลักสูตรปริญญาวิทยาศาสตรมหาบัณฑิต
สาขาวิชาฉายาเวชศาสตร์ ภาควิชารังสีวิทยา
คณะแพทยศาสตร์ จุฬาลงกรณ์มหาวิทยาลัย
ปีการศึกษา 2551

PERFORMANCE CHARACTERISTICS OF AUTOMATIC EXPOSURE CONTROL (AEC) SYSTEM FOR COMPUTED TOMOGRAPHY (CT) USING PHANTOM STUDY

Miss Supannee Pasongchun

A Thesis Submitted in Partial Fulfillment of the Requirements for the Degree of Master of Science Program in Medical Imaging
Department of Radiology
Faculty of Medicine
Chulalongkorn University
Academic Year 2008

Thesis Title	PERFORMANCE CHARACTERISTICS OF AUTOMATIC EXPOSURE CONTROL (AEC) SYSTEM FOR COMPUTED TOMOGRAPHY (CT) USING PHANTOM STUDY
By	Miss Supannee Pasongchun
Field of Study	Medical Imaging
Advisor	Associate Professor Anchali Krisanachinda, Ph.D.

Accepted by the Faculty of Medicine, Chulalongkorn University in Partial Fulfillment of the Requirements for the Master's Degree

.....Dean of the Faculty of Medicine
(Associate Professor Adisorn Patradul, M.D.)

THESIS COMMITTEE

..... Chairman
(Associate Professor Sukalaya Lerdlum, M.D.)

..... Advisor
(Associate Professor Anchali Krisanachinda, Ph.D.)

.....Examiner
(Assistant Professor Panruethai Trinavarat, M.D.)

.....External Examiner
(Professor Franco Milano, Ph.D.)

สุพรรณี ภาสองชั้น : การศึกษาการทำงานของระบบปรับปริมาณรังสีอัตโนมัติของเครื่องเอกซเรย์คอมพิวเตอร์ด้วยหุ่นจำลอง. (PERFORMANCE CHARACTERISTICS OF AUTOMATIC EXPOSURE CONTROL (AEC) SYSTEM FOR COMPUTED TOMOGRAPHY (CT) USING PHANTOM STUDY) อ.ที่ปรึกษาวิทยานิพนธ์หลัก : รศ.ดร.อัญชลี กฤษณจินดา, 78 หน้า.

ปัจจุบันการวินิจฉัยด้วยเครื่องเอกซเรย์คอมพิวเตอร์(ซีที) และจำนวนเครื่องได้มีเพิ่มมากขึ้นและเป็นผลให้ผู้ป่วยได้รับปริมาณรังสีเพิ่มขึ้นเมื่อเปรียบเทียบกับปริมาณรังสีจากการใช้เครื่องเอกซเรย์ทั่วไป เพื่อให้เกิดความเหมาะสมทั้งปริมาณรังสีและคุณภาพของภาพนั้น ผู้ผลิตได้เสนอวิธีลดปริมาณรังสีโดยใช้ระบบปรับรังสีอัตโนมัติ วัตถุประสงค์ของงานวิจัยนี้เพื่อศึกษาและประเมินการปฏิบัติงาน และคุณลักษณะเฉพาะของระบบอัตโนมัติ และระบบตั้งค่าต่างเพื่อศึกษาปริมาณรังสีซีทีดีไอและคุณภาพของภาพโดยใช้หุ่นจำลองรูปกรวยที่มีเส้นผ่านศูนย์กลางหลายขนาดซึ่งแทนขนาดต่างๆของช่องท้องของเด็ก

วิธีการ ทำการสแกนหุ่นจำลองรูปกรวยบรรจุวุ้นที่มีเส้นผ่านศูนย์กลางขนาด 10, 15, 20 และ 25 เซนติเมตรด้วยเครื่องซีที โดยใช้เทคนิคค่าเควีพี 80, 100 และ120 สำหรับระบบอัตโนมัติและระบบตั้งค่า ซึ่งเปลี่ยนค่ากระแสหลอด-วินาทีเป็น 50, 70, 90 และ110 บันทึกค่าปริมาณรังสีของซีทีดีไอปริมาตรและคำนวณค่าความแปรปรวนของภาพ รังสีแพทย์เป็นผู้ประเมินคุณภาพของภาพ โดยพิจารณาร่วมกับค่าปริมาณรังสีของซีทีดีไอ โดยมี 12 ภาพ ที่ใช้ระบบอัตโนมัติ และ 48 ภาพ ในระบบตั้งค่า

ปัจจัยที่มีอิทธิพลต่อคุณลักษณะเฉพาะในระบบอัตโนมัติคือ ค่ากระแสหลอด-วินาที ซึ่งอยู่ในช่วง 45-116 ที่ 80 เควีพี, 43-117 ที่ 100 เควีพี และ 43-117ที่ 120 เควีพี ตามลำดับ ค่าปริมาณรังสีของซีทีดีไอปริมาตรอยู่ในช่วง1.17-3.02, 2.15-5.85 และ 3.35-9.13 มิลลิเกรย์ และค่าความแปรปรวนของภาพ 9.36-28.42, 6.88-16.98และ 5.32-13.08 หน่วย สำหรับระบบตั้งค่า ค่าปริมาณรังสีซีทีดีไอปริมาตรคือ1.3, 1.82, 2.34 และ 2.86 มิลลิเกรย์ที่ 80 เควีพี, 2.5, 3.5, 4.5และ 5.5 มิลลิเกรย์ที่ 100 เควีพี และ 3.9, 5.46, 7.02 และ 8.58 มิลลิเกรย์ที่ 120 เควีพี และค่าความแปรปรวนของภาพ 5.68-41.68 หน่วยที่ 80 เควีพี, 4.0-24.4 หน่วยที่ 100 เควีพี และ 3.46-18.76 หน่วยที่ 120 เควีพี สำหรับคุณภาพของภาพประเมินโดยรังสีแพทย์คือ1=ไม่ยอมรับ, 2=ยอมรับ, 3=ดีและ 4=ดีมาก ระบบอัตโนมัติคะแนน 1 มี 16.7%, 2 มี 58.3%, 3 มี 25% และ 4 มี 0% ระบบตั้งค่า 1 มี 14.5%, 2 มี 37.5%, 3 มี 33.3% และ 4 มี 14.5% สาเหตุที่คุณภาพของภาพที่ใช้ระบบอัตโนมัติไม่มีภาพดีมากเนื่องจากจำนวนภาพมีเพียง 12 ภาพ และระบบอัตโนมัติพยายามปรับให้คุณภาพของภาพพอใช้ได้ โดยปริมาณรังสีไม่สูงเกินไป

ผลของระบบอัตโนมัติทั้งค่าปริมาณรังสีของซีทีดีไอปริมาตรและค่าความแปรปรวนของภาพจะเปลี่ยนแปลงตามขนาดของหุ่นจำลองโดยจะเพิ่มขึ้นตามขนาด ระบบตั้งค่ามีข้อจำกัดของค่าปริมาณรังสีของซีทีดีไอจะคงที่ในหุ่นจำลองทุกขนาด ดั้งนั้นได้ศึกษาความเหมาะสมของหุ่นจำลองขนาด 10, 15, 20 และ 25 เซนติเมตร โดยระบบอัตโนมัติควรใช้เควีพี 80, 80, 100 และ 120 ระบบตั้งค่าควรใช้เควีพี 80 /ค่ากระแสหลอด-วินาที 50, เควีพี 80 /ค่ากระแสหลอด-วินาที 70, เควีพี 100 /ค่ากระแสหลอด-วินาที 90 และ เควีพี 120 /ค่ากระแสหลอด-วินาที 70 ตามลำดับ จำเป็นจะต้องศึกษาคุณลักษณะดังกล่าวของเครื่องเอกซเรย์คอมพิวเตอร์ทุกเครื่องก่อนนำมาใช้ในผู้ป่วย

ภาควิชา รังสีวิทยา ลายมือชื่อนิสิต สุพรรณี ภาสองชั้น

สาขาวิชา ฉายาเวชศาสตร์ ลายมือชื่ออ.ที่ปรึกษาวิทยานิพนธ์หลัก อัญชลี กฤษณจินดา

ปีการศึกษา 2551

5074859430 : MAJOR MEDICAL IMAGING
KEYWORDS :MULTI-SLICE COMPUTED TOMOGRAPHY (MSCT) / AUTOMATIC EXPOSURE CONTROL(AEC) / IMAGE QUALITY /PEDIATRIC PHANTOM

SUPANNEE PASONGCHUN: PERFORMANCE CHARACTERISTICS OF AUTOMATIC EXPOSURE CONTROL (AEC) SYSTEM FOR COMPUTED TOMOGRAPHY (CT) USING PHANTOM STUDY. ADVISOR: ANCHALI KRISANACHIDA, Ph.D., 78 pp.

The number of CT examinations has increased as the growing number of the installed scanners. This resulted in the increased patient dose from the CT scan when compared to other radiographic examinations. In order to optimize the radiation dose from CT scan and maintain the image quality, several methods were proposed by the manufacturer and the users. One method to obtain the patient dose reduction from CT scan is the use of Automatic Exposure Control (AEC) system. The objective of this study is to evaluate the characteristics of AEC and non AEC systems on radiation dose ($CTDI_{vol}$) and image noise using an agar cone phantom of various diameters represent the pediatric abdomen.

A cone phantom diameters 10, 15, 20 and 25 cm, was scanned by a multi-slice computed tomography with the parameters of kVp at 80, 100 and 120 for AEC and non AEC, mAs at 50, 70, 90 and 110. Both systems were applied for each phantom diameter which $CTDI_{vol}$ and image noise were studied. The image quality of 12 AEC and 48 non AEC images had been assessed by the qualified radiologists.

The image quality scoring was related to the $CTDI_{vol}$. The AEC characteristic was studied on the effect of phantom sizes and the effective mAs. The range of effective mAs was 45-116 at 80 kVp, 43-117 at 100 kVp and 43-117 at 120 kVp respectively. The $CTDI_{vol}$ was 1.17-3.02, 2.15-5.85 and 3.35-9.13 mGy and image noise was 9.36-28.42, 6.88-16.98 and 5.32-13.08 HU for each kVp and diameter. For non AEC, the $CTDI_{vol}$ were 1.3, 1.82, 2.34 and 2.86 mGy at 80 kVp, 2.5, 3.5, 4.5 and 5.5 mGy at 100 kVp and 3.9, 5.46, 7.02 and 8.58 mGy at 120 kVp. The ranges of noise were 5.68-41.68 HU at 80 kVp, 4.0-24.4 HU at 100 kVp and 3.46-18.76 HU at 120 kVp. The qualitative image quality scored by a radiologist was 1- not acceptable, 2- acceptable, 3 - good and 4- very good. The result on AEC was: score 1 -16.7%, 2- 58.3%, 3- 25% and 4- 0% and non AEC the score was 1- 14.5%, 2- 37.5%, 3- 33.3% and 4- 14.5%. As the number of AEC image was less than non AEC, and the AEC system modulated mAs to optimal values, the percentage of very good quality is none.

The AEC system had influenced on the dose and noise of the phantom sizes. The limitation on the use of non AEC, the $CTDI_{vol}$ is constant at all phantom diameters and increases with increasing kVp. Therefore, the optimal protocols were set for both AEC and non AEC modes at each phantom diameter. For the diameters of 10, 15, 20, 25 cm the protocols are kVp 80, 80, 100 and 120 kVp for AEC mode and kVp 80/ mAs 50, kVp 80/ mAs 70, kVp 100/ mAs 90 and kVp 120/ mAs 70 for non AEC mode. The pediatric abdomen protocol should be studied for each CT system to optimize the patient dose and reasonable image quality.

Department : Radiology Student's Signature Supannee Pasongchun
Field of Study : Medical Imaging Advisor's Signature Anchali Kri
Academic Year : 2008

ACKNOWLEDGEMENTS

The success of this thesis could be attributed to the extensive support and assistance from my advisor, Assoc. Prof. Anchali Krisanachinda, Ph.D. and my co-advisor, Mr. Wallop Makmool, M.Sc.. I deeply thank them for their invaluable advices and guidance in this research.

I wish to deeply thank my thesis committee, Assoc. Prof. Sukalaya Lerdlum, M.D., M.Sc. and Assoc. Prof. Panruethai Trinavarat, M.D., Division of Diagnostic Radiology, Department of Radiology, Assoc. Prof. Sivalee Suriyapee, Chief Physicist at Division of Radiation Oncology, Department of Radiology, Faculty of Medicine, Chulalongkorn University, Professor Franco Milano, University of Florence, Italy and Assoc. Professor Katsumi Tsujioka, Fujita Health University, Japan, for their kindness, helpful and valuable suggestions.

I would like to deeply thank Assoc. Prof. Somjai Wangsuphachart, M.D., M.Sc., Head of Department of Radiology, Faculty of Medicine, Chulalongkorn University for her kindness, helpful and valuable suggestions.

I would like to thank Ms. Petcharleeya Suwanpradit, M.Sc., technologists, technicians and medical staffs in the Section of Computed Tomography, Department of Radiology, King Chulalongkorn Memorial Hospital, Thai Red Cross Society for their advices on the instrument and providing suggestions.

I would like to thank Mr.Taweap Sanghangthum, Mr.Sornjarod Oonsiri and staff at Division of Radiation Oncology, Department of Radiology, King Chulalongkorn Memorial Hospital, for their kindness in providing suggestions.

I would like to thank Mrs.Weeranuch Kitsukjit for her suggestion for the statistics in the research methodology.

I am grateful to all the lecturers and staff of Medical Imaging Department of Radiology Faculty Medicine, Chulalongkorn University, for supplying the knowledge in Medical Imaging.

Finally, I am grateful to my family for their financial support, valuable encouragement, entirely care and understanding for the entire course of study.

CONTENTS

Page

LIST OF TABLES

Table **Page**

LIST OF FIGURES

Figure **Page**

Figure **Page**

LIST OF ABBREVIATIONS

Abbreviation	Terms
2D	Two dimensions
3D	Three dimensions
A	Atomic mass
AAPM	American Association of Physicists in Medicine
AEC	Automatic Exposure Control
AP	Antero-posterior
cm	centimeter
cm^2	Square centimeter
CT	Computed tomography
CTDI	Computed Tomography Dose Index
$CTDI_{100}$	Computed Tomography Dose Index measured in air using ionization chamber
$CTDI_{100,c}$	Computed Tomography Dose Index measured at the centre of the phantom using ionization chamber
$CTDI_{100,p}$	Computed Tomography Dose Index measured at the periphery of the phantom using ionization chamber
$CTDI_{vol}$	Volume Computed Tomography Dose Index
$CTDI_w$	Weighted Computed Tomography Dose Index
CV	Coefficient of variation
DRL	Diagnostic Reference Level
DLP	Dose-length product
E	Effective Dose

Abbreviation	Terms
EC	European commission
FWHM	Full Width at Half Maximum
FOV	Field of view
ICRP	International Commission on Radiological Protection
HU	Hounsfield unit
ImPACT	Imaging Performance Assessment of Computed Tomography
Kg	Kilogram
keV	kiloelectronvolt
kV	kilovoltage
kVp	kilovolt-peak
LAT	Lateral
Lp/mm	Line pair per milli-meter
mA	Milliampere
mAs	milliampere-second
mAs_{QR}	quality reference milliampere second
mAs_{eff}	effective milliampere second
Eff.mAs	Effective mAs
Gy	gray
mGy	milligray
mGy.cm	milli-Gray.centimeter
mSv	millisievert
mm	millimeter
MSCT	Multi-Slice Computed Tomography

Abbreviation	Terms
MSAD	Multiple Scan Average Dose
MIP	Maximum Intensity Projection
MTF	Modulation Transfer Function
PMMA	Polymethylmethacrylate
R	Roentgen
ROI	Region of interest
Sv	Sievert
SD	Standard deviation
s	Second
QC	Quality Control
vs	Versus
Z	Atomic number
g/cm^3	gram per cubic centimeter
SPR	Scan Projection Radiograph
IAEA	International Atomic Energy Agency

CHAPTER I

INTRODUCTION

1.1 Background and Rationale

The introduction of computed tomography (CT) in the 1970s led to a revolution in medical imaging. A further dramatic increase in the use of CT in the diagnosis of a variety of pathologic conditions came with the introduction of the spiral CT in 1990 and multi-detector row CT scanner in 1998, resulting in a rapid scan benefit for children. Currently, about 10% of CT examinations were performed in pediatric patients, and the overall collective radiation dose to population is about 67% [1, 2]. The radiation dose from CT remains a major concern, especially in pediatric applications, because of the potential carcinogenic effects. Radiation dose is affected by several scanning parameters such as kVp, mAs, pitch and slice thickness. In addition, image quality changes noticeably according to the patient's body habitus. Image noise in CT is known to be inversely proportional to the square root of the dose to the detector [3, 4, 5]. Thus, there has been a tendency to increase of patient dose to avoid excessive noise on CT images.

Optimization consists of the acceptance of the dose and the image noise as much as permissible for diagnostic purposes. In practice, adjustment of the exposure level is performed manually by the operator, by adjusting the acquisition parameters to the body part studied, to the size and expected density resolution of the anatomic lesions and the patient's size.

Automatic exposure control (AEC) system has been developed and implemented on most recent CT system by manufacturers. The aim of the AEC is to improve the consistency of image quality and to control the absorbed dose. The first descriptions of real-time AEC system were reported at the end of the 1990s, but widespread implementation of this technique and effective use in daily practice are still very recent. In pediatric patients, two articles demonstrated a possible dose reduction of 26% to 43% with no loss of diagnostic quality [6, 7, 8] when AEC is used.

1.1.1 Automatic Exposure Control (AEC) methods [9]:

There are three methods for AEC developed by several manufactures. Those are,

1.1.1.1 Patient size AEC

The AEC system adjusts the tube current based upon the overall size of the patient as shown in figure 1(a). The same mA is used for an entire examination or scan series. The aim is to reduce the variation in image quality from patient to patient.

1.1.1.2 Automatic tube current adaptation to patient size along z-axis (Z-axis AEC)

The tube current is adjusted for each rotation of the x-ray tube as shown in figure 1(b), taking into account the variation of the attenuation along the patient's z-axis (along the scanner couch). The goal is to reduce the variation in image quality of images from the same series.

1.1.1.3 Angular tube current modulation (Rotation AEC)

The tube current is decreased rapidly (modulated) during the course of each rotation to compensate for differences in attenuation between lateral and AP projections as shown in figure 1(c). In general, lateral projections are more attenuation than AP, particularly in asymmetric regions of the body, such as the shoulders or pelvis.

These methods can be combined together as shown in figure 1(d).

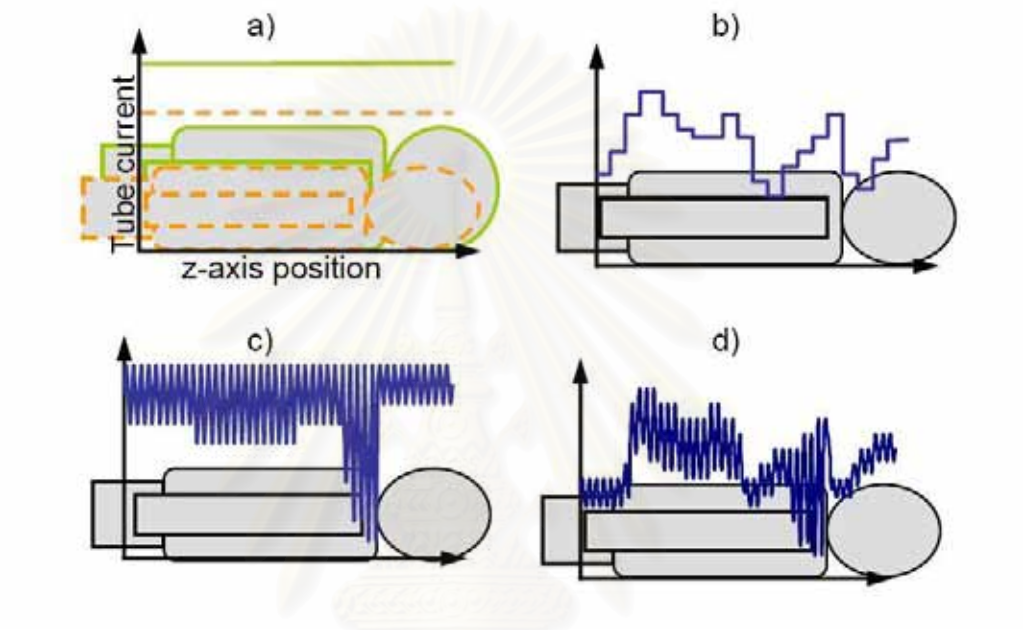

Figure1.1 Three levels of Automatic Exposure Control: a) patient size AEC, b) z-axis AEC, c) rotation AEC, d) combined effects of three levels of AEC.

Image noise is affected by rotational AEC in a different way to patient and z-axis AEC. Noise in any CT image is a function of the uncertainty of all the measurements that contribute to each pixel. The attenuation measurements with the greatest effect upon image noise are those with the greatest uncertainty, these are the ones where the fewest number of x-rays reach the detectors. Rotational AEC attempts to reduce the variation in uncertainty of attenuation measurements by increasing the tube current through the most attenuating projection angles, and reducing the mA where the attenuation is lowest.

As AEC has not been implemented for pediatric CT imaging at King Chulalongkorn Memorial Hospital, it is interesting to study the effect of AEC on pediatric phantom and technical factors on image quality and dose.

In this study, the performance characteristics of automatic exposure control (AEC) system for Siemens Sensation 16 MSCT using conical phantom contained agar will be studied for radiation dose and image noise as well as the effects in using routine abdomen CT protocol.

1.2 Research Objectives

1.2.1 To study the characteristics of AEC system in pediatric CT using phantom.

1.2.2 To study the difference in radiation dose and image noise when using AEC and non AEC systems.

CHAPTER II

REVIEW OF RELATED LITERATURES

2.1 Theory

2.1.1 Principles of Computed Tomography [10]

The CT scanner is a device using an X-ray source which can be used to give precise information on the attenuation properties of a thin sectional volume of the body. The configuration and image production processes are found extensively in the literature. The basic elements of the CT scanner include the X-ray tube and the detector or detector array located in the gantry and known as the data acquisition system, the image processing system, and the image display system. The X-ray tube rotates around the patient producing a tightly collimated X-ray radiation photon beam. Once attenuated by the patient the attenuated beam strikes the detectors which convert the photon intensity to a digital signal. Multiple profiles of patient attenuation are collected.

2.1.2 Historical Development of Computed Tomography [10, 11]

Each change in the fundamental CT tube-detector structure is known as a CT generations. The CT generation has changed from the first introduced in 1972 up to the fifth in more recent years. The generation development has improved acquisition time and image quality.

2.1.2.1 The first and second generation scanners

The first generation scanner was based on parallel beam geometry and the translate scanning motion. It used a single highly collimated X-ray beam (pencil beam) and one or two detectors translated across the patient collecting transmission readings (figure 2.1A). This was done for 180° around the patient. This first generation scanner took 4.5 to 5.5 minutes to produce a complete scan of the head. The major problem for this generation is patient throughput, motion artifacts caused by the patient, and poor image quality.

Second-generation scanners are based on a small fan beam geometry and translate rotate motion (figure 2.1B). This method is referred to as rectilinear multiple pencil beam scanning and the path traced by the X-ray tube during the scanning is the same as first generation that is 180°. The scan motion and increasing detector numbers reduced the scanning time to 20 to 60 seconds.

The first and second generation scanners are no longer in use. They have been replaced by third and fourth generation scanners

2.1.2.2 The third and fourth generation scanners

Third generation scanners employ rotate-rotate configuration based on a fan beam geometry with no translation and complete rotation of the X-ray tube and detectors (figure 2.1C). The X-ray tube is coupled to a curved detector array that

subtends an arc of about 30° to 40° from the apex of the fan located at the X-ray tube. The fan beam geometry rotates continuously around the patient for 360°. The minimum scan time is 1 to 4 seconds. The fourth generation scanners are based on fan beam geometry and complete rotation of the X-ray tube around a stationary 360° ring of detectors (figure 2.1D). The number of detectors in such a scanner varies from about 300 to 4000. The scan time ranges from 2 to 8 seconds.

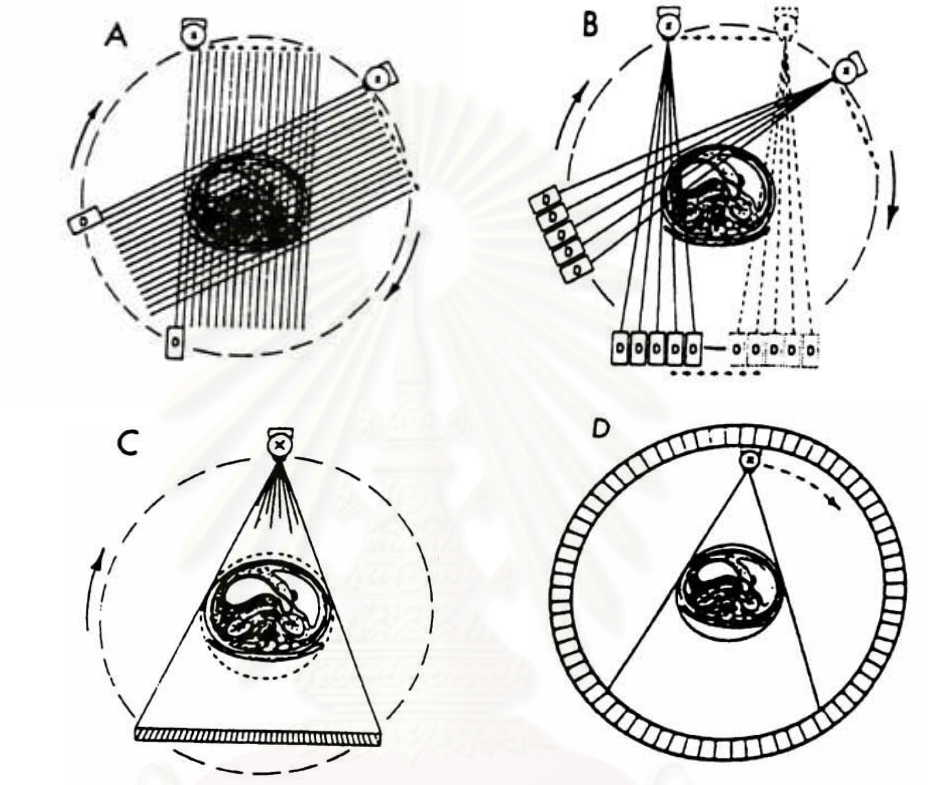

Figure 2.1: Development of computed tomography generation. (A) The first generation CT using translate-rotate principle. (B) Second generation as a rectilinear multiple pencil beam scanning system. (C) The third generation CT using rotate-rotate principle. (D) The fourth generation CT using rotate-stationary principle.

2.1.2.3 The fifth generation (Electron beam scanners)

Electron beam scanners, also known as the fifth CT generation, have been developed primarily for high speed CT scanning (figure 2.2) and use a special configuration. These scanners incorporate a semicircular tungsten target ring within the gantry. An electron beam with energy of 130 keV strikes the target ring as it is swept around the gantry thus the X-ray focal spot moves around the patient. The stationary semicircular bank of detectors records the X-ray transmission in a fashion similar to that of a fourth-generation scanner. By using four target rings and two detector banks, eight slices of the patient may be imaged allowing acquisition of about 17 images per second. This capability allows images of high motion structures such as the heart to be visualized in coronary studies.

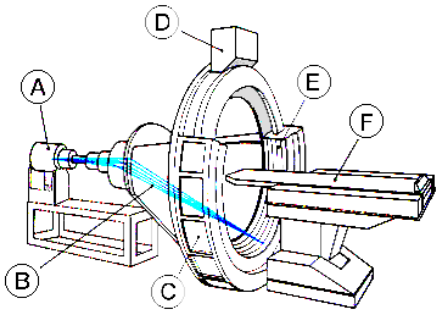

Figure 2.2: Electron Beam CT illustrates the electron gun (A), electron beam (B), self contained internal cooling system (C), data acquisition system (D), target ring (E), precise high-speed couch motion (F).

2.1.2.4 The sixth generation

In the early 1990s, the design of the third and fourth generation scanners evolved to incorporate slip ring technology. A slip ring is a circular contract with sliding brushes that allows the gantry to rotate continually, untethered by wires. The use of slip-ring technology eliminated the inertial limitations at the end of each slice acquisition, and the rotating gantry was free to rotate continuously throughout the entire patient examination. This design made it possible to achieve greater rotational velocities than with systems not using a slip ring, allowing shorter scan times. Helical CT (also inaccurately called spiral CT) scanners acquire data while the table is moving; as a result, the x-ray source moves in a helical pattern around the patient being scanned. Helical CT scanners use either third- and fourth-generation slip-ring designs. By avoiding the time required to translate the patient table, the total scan time required to image the patient can be much shorter. Consequently, helical scanning allows the use of less contrast agent and increase patient throughput. In some instances the entire scan can be performed within a single breath-hold of the patient, avoiding inconsistent levels of inspiration. The advent of helical scanning has introduced many different considerations for data acquisition. In order to produce reconstructions of planar sections of the patient, the raw data from the helical data set are interpolated to approximate the acquisition of planar reconstruction data. The speed of the table motion relative to the rotation of the CT gantry is a very important consideration, and the pitch is a parameter that describes this relationship.

2.1.2.5 The seventh generation

X-ray tubes designed for CT have impressive heat storage and cooling capabilities, although the instantaneous production of x-rays (i.e., x-rays per mAs) is constrained by the physics governing x-ray production. An approach to overcoming x-ray tube output limitations is to makes better use of the x-rays that are produced by the x-ray tube. When multiple detector arrays were used, the collimator spacing was wider and therefore more of the x-ray that was produced by the x-ray tube was used in producing image data. With conventional, single detector array scanners, opening up the collimator increases the slice thickness, which was good for improving the utilization of the x-ray beam but reduce spatial resolution in the slice thickness dimension. With the introduction of multiple detector arrays, the slice thickness was determined by the detector size and not by the collimator.

2.1.3 Multi Slice Computed Tomography (MSCT)

The simultaneous introduction in 1998 of computed tomography with multislice acquisition and half-second rotation time allowed major advances in CT imaging. Continuing technical developments have resulted in a reduction of the rotation time to 0.4 seconds and an increase in the number of simultaneously acquired slices to 16. Multislice CT (MSCT) with sub-second rotation times allows for the scanning of long ranges (advantageous in, for example, peripheral multislice CTA), for shorter scan times (advantageous in, for example, pediatric CT and trauma), and for a reduction in movement artefacts (as, for example, in ECG gated cardiac CT). With the reconstructed thin axial sections provided by MSCT, a near-isotropic 3-dimensional volume with sub-millimeter sized voxels can be constructed, that is well-suited for review on advanced 3D workstations. This is particularly true for 16 (or more) slice scanners. Review of (often thicker) axial images can be performed in cine mode and in addition sophisticated image reviewing on dedicated workstations allows for e.g. 2D multiplanar and curved planar reformatting (MPR and CPR), maximum intensity projection (MIP) and 3D volume rendering.

MSCT accounts for nearly 50 % of the resultant collective dose from diagnostic radiology in European Union. Special measures are consequently required to ensure optimization of performance in CT, including MSCT, and effective patient protection. The requirement for special attention to radiation protection in computed tomography was formalized in European legislation, which demands that member states pay special attention to radiation protection in computed tomography and in pediatric radiology in comparison with conventional computed tomography, acquisition techniques, contrast enhancement and reconstruction.

2.1.3.1 European Quality Criteria for MSCT

The quality criteria concept, as developed for conventional x-ray examinations of adult and pediatric patients and for computed tomography of adult patients by the European Commission's (EC) research actions, has proved to be an effective method for optimizing the use of ionizing radiation in medical imaging procedures. The purpose of the quality criteria for CT published in 2000 was to provide an operational framework for radiation protection initiatives for this modality, in which technical parameters required for image quality were considered in relation to patient dose.

A drawback of the publication in the year 2000 is that it deals only with single slice CT scanners. The present document provides an update of the European CT quality criteria for multislice scanners operating with 4 to 16 active acquisition channels

2.1.3.2 Differences between Multi- and Single-slice Scanners [12]

The single detector in a multi-row, solid state detector array are separated by narrow strips (septa) which are not sensitive to radiation and therefore do not contribute to detector signal. Due to the large number of strip, these inactive zones result in minor or major geometrical losses, depending on the design of the detector array. In addition, further losses occur due to a decrease in sensitivity at the edges of each row that results from cutting the scintillator crystal. In contrast to a single-row detector array whose width can be larger than the maximum slice thickness (figure 2.3) the edges of the rows in a multi-row detector array are located inside the beam.

Due to both these effects- separating strips and decreased sensitivity- the net efficiency of a solid state detector array is further decreased.

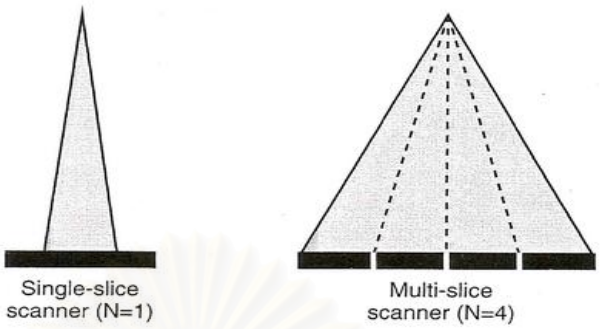

Figure 2.3 MSCT scanner, with simultaneous scanning of 4 slices, compared with a conventional single-slice scanner.

Another design of a multi-row detector array, which employs only haft the number of rows, is illustrated in figure 2.4.(a) When small slices are to be acquired, only the central portion of the array needs to be used. It is therefore not necessary to use narrow rows also in the outer portions of the array, in order to allow simultaneous acquisition of four slices each of 5 mm thickness. This design is not only less expensive, but also geometrically more efficient.

In the generation of 16 slice scanners, which was introduced at the RSNA meeting in 2001, hybrid detector arrays are used (figure 2.4. b). These employ 16 rows of detectors of small width (e.g. each of 0.75 mm), completed by four rows of detectors with greater width (e.g. 1.5 mm) on either side. This design allows the simultaneous scanning of 16 slice, each 0.75 mm wide, or 16 slice each 1.5 mm wide. The latter is achieved by grouping together in pairs the 0.75 mm wide rows in the inner part of the array.

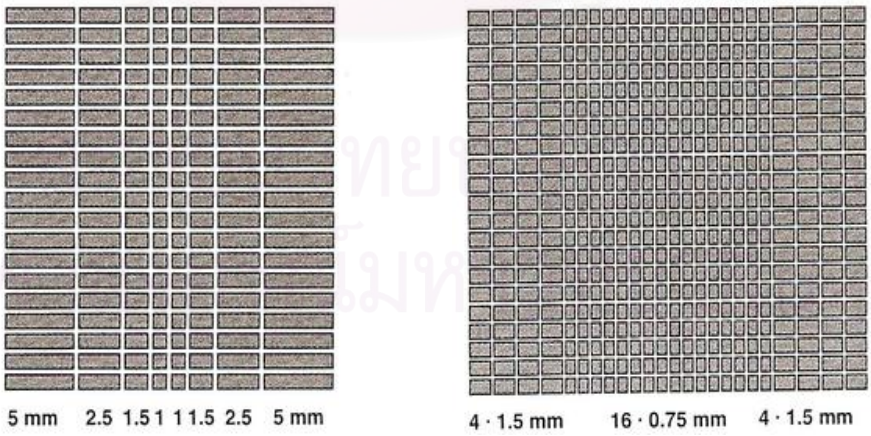

a) b)

Figure 2.4 a) A 20 mm wide multi-row detector array, for simultaneous scanning of 4 slice each to 5 mm thick., b**)** A 24 mm wide hybrid multi-row detector array for simultaneous scanning of 16 slice each to 0.75 and 1.5 mm thick.

The primary determinant of multi-slice scanners is not the number of detector row, but merely the number of slices N which are acquired simultaneously. The speed needed to cover a given volume is improved by a factor of up to N. The reason why N was initially limited to 4 were the increased amount of data to be acquired and transferred simultaneously, and the occurrence of cone beam artifacts. The more slices that are acquired simultaneously, the less these artifacts can be suppressed with the conventional fan-beam approach. Once the appropriate cone beam algorithms (or at least advanced fan beam-like approaches) and the increased computation power needed for this class f algorithms became available. Such developments will continue over the next few years and will lead in the medium-term to extended cone beam CT.

2.1.4 Automatic Exposure Control (AEC) system [9]

On non-AEC based systems, the user sets the tube current for each examination, either through selection of a pre-set protocol, or by manually entering an mA or mAs value. For AEC systems to operate, a method is needed for the user to set the desired image quality level. A number of approaches are currently used, each of which has its own advantages and disadvantages.

The general aim of an AEC system for CT is to significantly reduce, or eliminate variations in image quality between different images. This also reduces the variation in radiation doses to different sized patient cross sections. On present systems, this is achieved through the control of the x-ray tube current to achieve the required level of image noise.

2.1.4.1 Methods for AEC system control

a).Standard deviation based AEC control

Using this method, the user controls the AEC by specifying image quality in terms of the resultant standard deviation (SD) of pixel values. Setting a high SD value gives a noisy image; low SD settings give low noise images. The scanner aims to set the tube current that is required to achieve the requested standard deviation on an image by image basis.

One advantage of this method is that the image quality resulting from protocols from different scanners can be compared more easily, although when comparing settings from different manufacturers it is important to be aware of differences in the implementation of the systems.

Using an SD based system, the AEC is controlled by setting image quality, rather than using tube current, which is a radiation exposure related measure. Users will have to familiarize themselves with this new way of working with the scanner, as an understanding of the standard deviation of an image is not intuitive. It is important to ensure that the SD chosen is appropriate for the clinical task. It would easily be possible to enter a SD which is lower than would be needed, resulting in higher patient doses than the ones achieved without AEC. Users also need to understand that image noise is inversely proportional to the square of the tube current, so halving the SD results in an increase in the mA, and therefore the patient dose, by a factor 4.

b). Reference mAs AEC control

This method of AEC control uses the familiar concept of setting an mA (or mAs) related value for a scanner protocol, in this case a 'reference' mAs is used. This is the value that would be used on an average sized patient. The AEC system assesses the size of the patient cross-section being scanned, and adjusts the tube current relative to the reference value.

The reference mAs concept permits more flexible adjustment of tube current than with standard deviation AEC controls. With SD based systems, the AEC response to different patient sizes is pre-defined, because the aim is always to keep the image noise constant. Reference mAs systems can vary their response, depending on the image quality requirements. For example, it is possible to 'under correct' for changes in patient size, so that images of small patients are less noisy than the standard patient, and those for larger patients are noisier than the standard. Smaller patients generally require better image quality than larger patients, who have a different fat distribution, making the organs easier to visualize.

It is not as straightforward to make comparisons between reference mAs protocols as it is with SD based techniques. This is because the tube current that is used for a standard patient depends upon scanner design features, such as beam filtration and scanner geometry, as well as the definition of a standard patient. However, users are generally familiar with typical mAs values for their scanners, and the move to equivalent mAs is an easier step to make than to an SD based AEC.

c). Reference image AEC control

The third approach that is currently used for controlling AEC systems is to use a 'reference image' that has previously been scanned and judged to be of appropriate quality for a particular clinical task. The scanner then attempts to adjust the tube current to match the noise in the reference image. The main advantage of this system is that when setting it up for use, the required image quality is expressed using an existing clinical image, rather than an abstract value of standard deviation.

One possible drawback is that the temptation will be to pick a 'pretty' image, with low noise rather than one which has been judged to be good enough for the task. This could potentially lead to the system attempting to match higher quality images than are needed and using higher doses than are necessary. It is also difficult to compare scan protocols, even for two scanners of the same model, as there is no value associated with the image quality in the reference image.

2.1.4.2 Approaches for AEC operation

Whatever method the AEC uses to control the exposure or image quality level, there needs to be a way for the system to assess the attenuation of each patient, and calculate the tube current required.

a) Patient size and z-axis AEC

Scan projection radiographs (SPRs, known as scout, scanogram or topogram views) are the main way that AEC systems assess the attenuation of the patient in order to set the tube current. Figure 2.5 shows an AP and a lateral SPR view from the

same patient, overlaid with a graph of the summed attenuation of the patient at each z-axis position. This information can be used as the basis for patient and z-axis AEC. In practice, AEC systems tend to operate using a single SPR view, to be compatible with existing clinical practice.

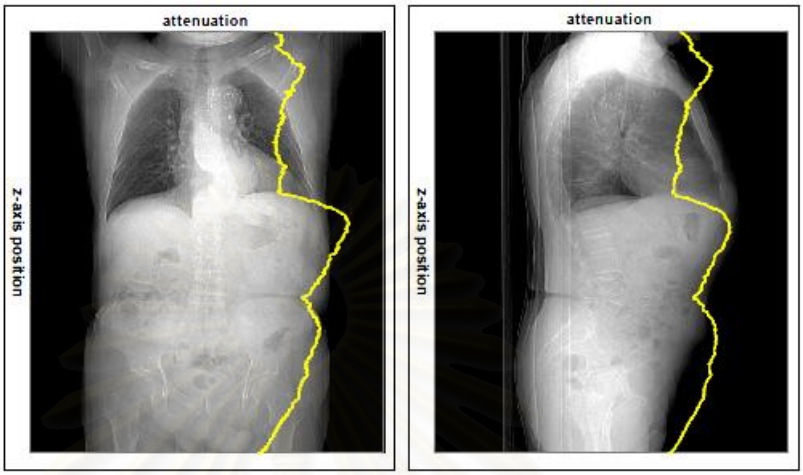

Figure 2.5 Patient attenuation measured along the z-axis from AP and lateral SPR views

b). Rotational AEC

In order to supply the information required for rotational AEC, data is required on how asymmetric the patient is at each position. It is possible to make estimates of this from the pattern of the attenuation profile across the patient at each z-axis position, and vary the tube current accordingly.

Another way of gaining information on the patient's rotational symmetry is to use feedback from the measurements during the course of the CT scan. Changes in the patient profile generally occur gradually along the z-axis, so the shape of the attenuation profile at each angle during each rotation can be used to control the tube current during the next rotation. In practice, the feedback can come from the scan data acquired in the previous 180° in order to reduce the lag between the change in the patient's shape, and the system's response. It is possible to use a predefined function, such as a sine wave, to vary the current between the maximum and minimum value in each rotation.

2.1.4.3 AEC system for CARE Dose 4D [13]

1). CARE Dose 4D combines two types of tube current modulation :

a. Automatic tube current adaptation to patient size along z-axis (Z-axis AEC)

Based on a single topogram (AP or lateral) the attenuation profile along the patient's long axis is measured in direction of the projection and estimated for the perpendicular direction by a sophisticated algorithm.

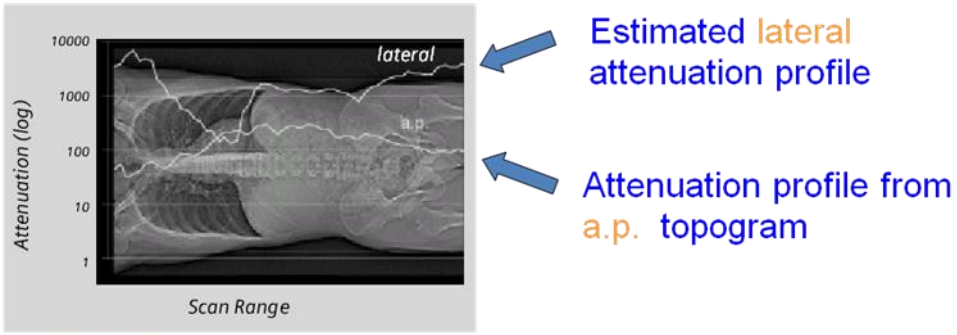

(Courtesy of Siemens)

Figure 2.6 Z-axis AEC

Based on these attenuation profiles, axial tube current profile (lateral or AP) are calculated. The correlation between attenuation and tube current is defined by an analytical function which results in an optimum of dose and image noise in every slice of the scan.

The tube current is adjusted for each rotation of the x-ray tube, taking into account the variation of the attenuation along the patient's z-axis (along the scanner couch). The goal is to reduce the variation in image quality of images from the same series.

b. Angular tube current modulation (Rotation AEC)

Since changes in the patient profile occur gradually along the z-axis, the shape of the attenuation profile at each angle during each rotation can be used to control the tube current during the next rotation.

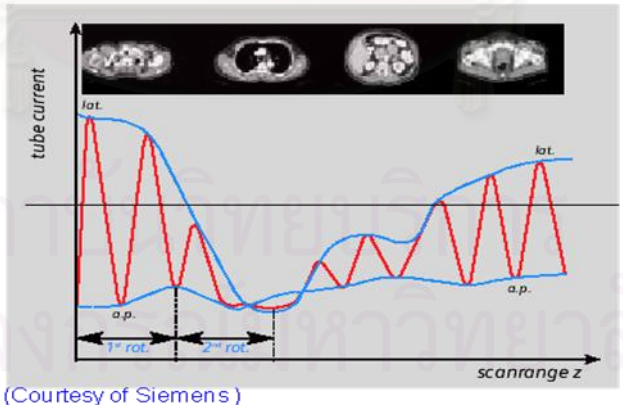

(Courtesy of Siemens)

Figure 2.7 Rotation AEC

The tube current is decreased rapidly (modulated) during the course of each rotation to compensate for differences in attenuation between lateral and AP projections. In general, lateral projections are more attenuation than AP, particularly in asymmetric regions of the body, such as the shoulders or pelvis.

AEC constitutes a method that aims to improve the consistency of image quality among patients with different body size and to optimize the absorbed dose by modulating tube current according to a patient's attenuation. The method is based on a combination of automatic tube current adaptation to the patient's body size and anatomic shape, and on-line tube current modulation for each tube rotation. Based on a single anterior-posterior (AP) or lateral (LAT) topogram, the attenuation profile along the patient's z-axis is measured in the direction of projection. The corresponding attenuation profile in the perpendicular direction of projection (LAT or AP) is estimated by a sophisticated algorithm. Based on the above two attenuation profile, the axial tube current profiles are calculated and applied during the scan. The angular attenuation values (x-y plane) are online read out as a function of the rotation angle and the tube current is adapted accordingly in real time to achieve an optimum distribution of the x-ray intensity for every viewing angle. The latter process provides images with a more uniform level of image noise across the field of view at a lower average tube current. Detailed information on the operation characteristics of z-axis and angular (x, y) on-line tube current modulation can be found elsewhere [13-16].

2). Scanning with CARE dose 4D [13-15]

With the settings of "Image Reference mAs" properly predefined, no further adjustment of the tube current has to be made to perform a scan. CARE Dose 4D automatically adapts the tube current to different patient size and anatomic shapes, but it ignores metal implants.

For an accurate mAs adaptation to the patient's size and body shape with CARE Dose 4D the patient should be carefully centered in the scan field.

When using protocol with CARE Dose 4D for other than the body regions they are designed for, the image quality should be carefully evaluated.

As CARE Dose 4D determines the (eff.) mAs for every slice from the topogram, a topogram must be performed to use CARE Dose 4D. For an optimum image quality the kV setting for the topogram and the subsequent scans should be identical. The range of the scan should not exceed the range of the topogram.

In this study, AEC is accomplished by means of the CARE Dose 4D implementation in a Somatom Sensation 16 MSCT scanner (software version syngo, Siemens, Germany) as shown in figure 3.3. An image quality reference milliampere sec (mAs_{QR}) value is predefined for every scan protocol. This value corresponds to the effective millampere sec (mAs_{eff}) value that the operator would apply for a "reference patient" during the scan without the use of the AEC. The mAs_{eff} value is defined as product of the tube current (mA) and the tube rotation time (s) divided by the pitch (p). The pitch is defined as the ratio between the table feed per rotation and x-ray beam width. The "reference patient" is defined s a typical adult weighing 70 kg to 80 kg (for adult protocol), or as a 5-year old typical child weighing 20 kg (for pediatric protocol). The operator is advised to keep the mAs_{QR} constant regardless of the individual patient size or age and adjust it only if image quality needs to be changed. The AEC software allows the use of different modulation strengths for slim and obese patients. By default, the modulation strength was set by the manufacturer to the "average decrease" for slim and "average increase" for obese patients. Being the default, this setting is expected to be followed in the everyday clinical practice by most institutions.

2.1.5 Dosimetry in MSCT [12, 18, 19]

2.1.5.1 Radiation Dose Specific to CT (Radiation Dose Measures)

The reason for different dose descriptors for CT and the methods of dose measurement in CT will be explained. The dose quantities specific to CT are:

- Computed Tomography Dose Index in air (CTDI in air)
- Weighted Computed Tomography Dose Index ($CTDI_w$)
- Volume Computed Tomography Dose Index ($CTDI_{vol}$)
- Dose-length product (DLP)
- Effective Dose (E)

a). Requirement for different dose descriptors

The dose distributed in CT examinations differs in several ways compared to general radiography First, the dose is equally distributed in the scanning plane as the patient is equally irradiated from all directions during a complete 360°, X-ray tube rotation along the x-y axis (figure 2.8). Second, the CT dose is also distributed along the patient z axis (plane AB). In this direction, radiation is not only deposited in the collimated area but also in its neighbourhood. The latter phenomenon is due to the penumbra and the divergence of the radiation beam (Figure 2.8 – insert). When multiple adjacent scans are performed this penumbra (radiation profile tail) will contribute to the area being irradiated and create additional absorbed dose. Third, CT may use several series in an examination, thus the same volume may be irradiated several times increasing the dose.

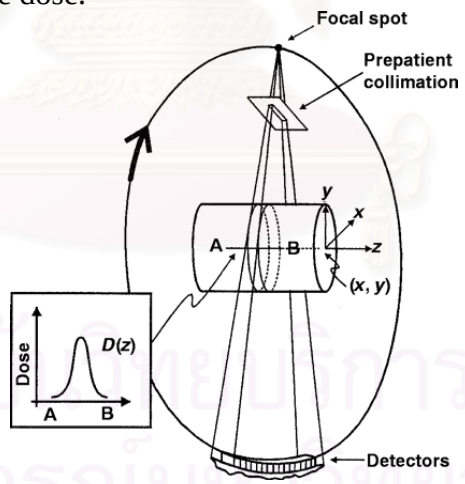

Figure 2.8 Configuration of CT system shows X-ray beam collimation along z-axis (line AB) through CTDI phantom. Insert indicates the dose profile measured along line AB.

CT dose quantities can be divided into two categories, as local dose and integral dose. Local dose quantities are indicators of the intensity of the radiation inside the limits of the irradiated body region for example CTDI and organ dose. The integral dose quantities are descriptors of the total amount of radiation absorbed during an examination by taking into account the extent of the body region. This category includes dose length product and effective dose.

b). CTDI measurement in air

The dose free-in-air ($CTDI_{air}$) can be measured by placing the detector at the isocentre of the scanner with its axis aligned to the axis of rotation. The detector must be clamped and held by a stand and extend beyond the end of the table in order to exclude attenuation of the beam by the table (figure 2.9). The marker at the centre of the detector length must coincide with the centre of the fan beam. The position of the detector is checked by performing a scan or by making use of the laser pointer. The use of a spirit level and visualization are also important to ensure that there is no rotation of the detector. Readings are obtained for selected scanner settings according to a measurement protocol, with variables such as tube potential, tube current, exposure time, rotation angle and slice thickness. The beam filtration selected and the total beam filtration for the central portion of the fan beam must also be recorded. The dosimeter reading is displayed in dose length product (DLP) mGy.cm. The result from the measurement, both CTDI in air ($CTDI_{air}$) and normalized CTDI in air ($_nCTDI_{air}$) can be calculated using equation 2.1 and 2.2 below,

$$CTDI_{air} = DLP_{air} / N.h \quad (mGy) \tag{2.1}$$

$$_nCTDI_{air} = CTDI_{air} / Q \quad (mGy.mAs^{-1}) \tag{2.2}$$

Where, N is number of slices scanned, h is nominal slice thickness in cm, Q is the mAs product that was used to measure CTDI, and DLP_{air} is dosimeter reading.

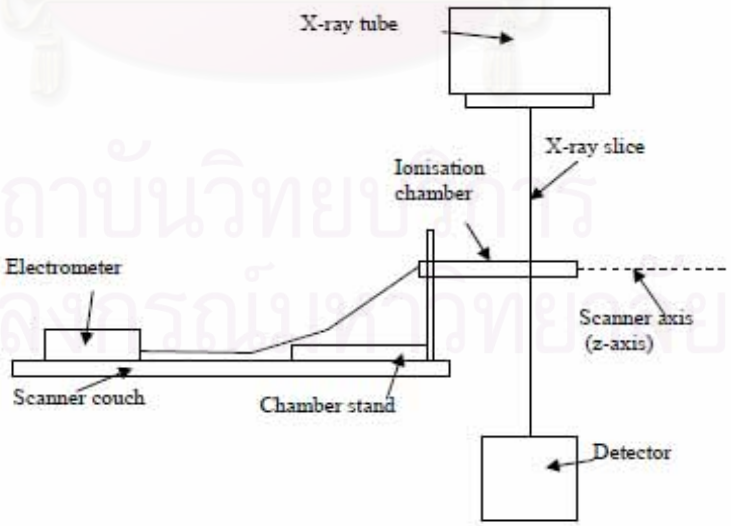

Figure 2.9 Arrangement of the ionization chamber for CTDI measurement in air.

c). CTDI measurement using phantoms

There are two standard phantoms used to make measurements of the CTDI (figure 2.10). A small cylindrical phantom, 15 cm in length with a diameter of 16 cm, is used for the head, neck and children. Another phantom of the same length but with a diameter of 32 cm represents the adult trunk. These phantoms are made of polymethyl methacrylate (PMMA) with five sockets that will accept insertion of the pencil ionization chamber. There is one hole at the centre and the four others are 1 cm below the phantom surface, each 90° apart from its neighbor and located at 3, 6, 9, and 12 o'clock. The inserts are 1 cm in diameter and 15 cm in length so that the ionization chamber fits perfectly in the holes.

When the CTDI measurement in a phantom is made, a pencil ionization chamber is inserted into one of the holes and is connected to an electrometer. Other holes remain fitted with their inserts. The central dose measurement is made three times to get an average. For the peripheral value ($CTDI_{100,P}$), the mean value of the measurements is made at 3, 6, 9, and 12 o'clock locations as calculated in equation 2.3.

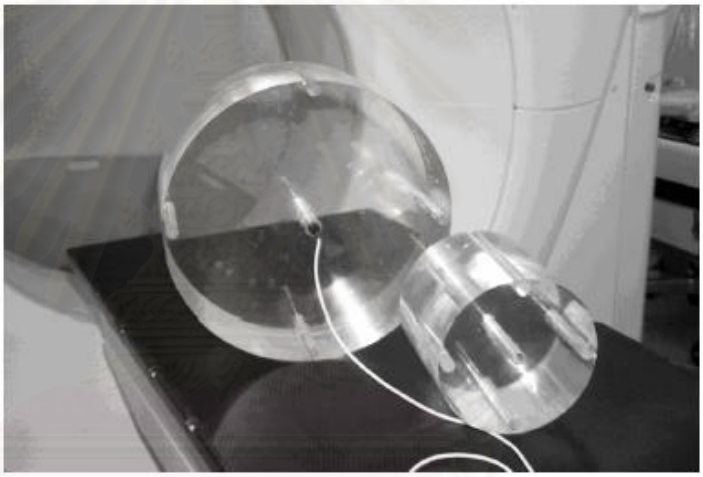

Figure 2.10 A body (large) and head (small) phantom for measurement of CT Dose Index. Pencil ionization chamber is inserted in the centre of the body phantom.

$$CTDI_{100,p} = 1/4 \sum_{i=3}^{12} CTDI_{100,p} \quad \text{(Gy)} \qquad (2.3)$$

where $CTDI_{100,p}$ is the dose measured at the phantom periphery.

In order to get $CTDI_{100,w}$ appropriate quantities can be replaced as in equation 1 and for ${}_nCTDI_{100,w}$ as in equation 2.2 Further, the average of peripheral and central values can be calculated using equation 2.4,

$$CTDI_w = (1/3)(CTDI_{100})_{center} + (2/3)(CTDI_{100})_{periphery} \quad \text{(Gy)} \qquad (2.4)$$

where $CTDI_{100,c}$ and $CTDI_{100,p}$ are dose measured at the phantom centre and at the periphery respectively.

d). Specific Dose unit for CT

The currently accepted appropriate descriptor for CT dose is the *Computed Tomography Dose Index* (CTDI). This is a local dose descriptor of dose output for scanners measured in air at the centre of rotation. The CTDI is defined as the radiation dose, normalized to beam width, measured from 100 mm length of a pencil ionization chamber.

$$CTDI_{100} = (1/NT) \int_{-5cm}^{5cm} D_{series}(Z)dz \qquad (mGy) \qquad (2.5)$$

where D(z) absorbed dose relative to location along the z axis; N is the number of acquired sections per scan (or the number of data channels used during acquisition) and T is the nominal width of each acquired section (product of NT is also known as beam collimation).

Specific imaging protocols also include the pitch as a factor, thus in consideration of that factor, another descriptor had been created. Those are $CTDI_{vol}$ or $CTDI_{W,eff}$. It is defined as

$$CTDI_{vol} = CTDI_{w} \cdot NT/I \qquad (mGy) \qquad (2.6)$$

where *N* and *T* are defined in equation 2.5 and represent the total collimated width of the X-ray beam and *I* is the table increment per rotation for helical scan or spacing between acquisition for axial scans.

As pitch is one of the parameters in spiral CT. Pitch is defined as table distance travelled in one 360° rotation over total collimated width of the X-ray beam, while in conventional CT it is defined as table increment over slice thickness. Pitch can be calculated by the equation 2.7.

$$Pitch = I/NT \qquad (2.7)$$

Thus equation 2.6 can be rewritten as,

$$CTDI_{vol} = CTDI_{w}/pitch \qquad (mGy) \qquad (2.8)$$

$$CTDI_{w} = CTDI_{vol} \text{ x pitch} \qquad (mGy) \qquad (2.9)$$

In describing the exposure distribution along the z axis another descriptor known as *Dose Length Product (DLP)* effective dose value without taking account of tissue weighting factor. The DLP is expressed in units of mGy.cm and given in the equation below,

$$DLP = CTDI_{vol} \cdot \text{scan length} \qquad (mGy.cm) \qquad (2.10)$$

The effective dose (E) is the most relevant quantity in which to express the effect and compare the dose absorbed in patients from different imaging procedures. The calculation of effective dose

$$E = \sum_T (W_T \cdot W_R \cdot D_{T,R}), \qquad (Sv) \qquad (2.11)$$

where E is the effective dose, W_T is the tissue-weighting factor, W_R is the radiation-weighting coefficient (1 for x rays), $D_{T,R}$ is the average absorbed dose to tissue T, T is the subscript for each radiosensitive tissue, and R is the subscript for each type of radiation (here, only x rays are present). The weighting factors are set for each radiosensitive organ in Publication 60 of the International Commission on Radiological Protection (ICRP). Effective dose is measured in sieverts (Sv) or rems. The conversion between sieverts and rems is 100 rem = 1 Sv.

2.1.5.2 Factors that influence radiation dose CT

In general, there are some factors that have a direct influence on radiation dose, such as the x-ray beam energy (kilovolt peak), tube current (in milliamperes), rotation or exposure time, section thickness, object thickness or attenuation, pitch and/or spacing, dose reduction techniques such as tube current variation or modulation, and distance from the x-ray tube to isocenter. In addition, there are some factors that have an indirect effect on radiation dose those factors that have a direct influence on image quality, but no direct effect on radiation dose; for example, the reconstruction filter. Choices of these parameters may influence an operator to change settings that do directly influence radiation dose. These factors are discussed in this section.

a). Beam Energy

The energy of the x-ray beam has a direct influence on patient radiation dose. This is selected by the operator (technologist) when the kilovolt peak is chosen for the scan. However, it is also influenced by the filtration selected for the scan. On some scanners, the selection of filtration is explicit; for others, it is implied (e.g., by selection of the scan field of view [SFOV]). The influence of beam energy when all other technical parameters are held constant and the kilovolt peak is increased on a single-detector CT scanner, the $CTDI_w$ values also increase for both the head and body CTDI phantoms. For example, when the kilovolt peak was increased from 120 to 140 on a CT/i scanner (GE Medical Systems, Milwaukee, Wisconsin USA), the $CTDI_w$ increase was 37.5% for the head phantom and 39% for the body phantom.

b). Photon Fluence

The photon fluence is determined by the quantity of electrons that hit the target and can be controlled by adjusting mAs. The photon fluence also has a direct influence on the patient radiation dose. The radiation dose is directly proportional to the mAs value. When all other factors remain constant, the $CTDI_W$ values increase linearly with mAs.

c). Pitch Factor

Pitch is defined as the table distance travelled in one 360° rotation over the total collimated width of the X-ray beam, while in conventional CT it is defined as table increment over slice thickness. Pitch has a direct influence on patient radiation dose. As pitch increases, the time to cover irradiated volume will be decreased. As a standard setting in CT scanning, table feed is equal to slice thickness. This means the pitch is equal to 1. However, if pitch is less than 1, i.e. the slices overlap, the dose is increased. In contrast, radiation exposure can be significantly reduced if a pitch factor of more than 1 is applied. The descriptor which indicates the effect of pitch is $CTDI_{vol}$.

d). X-ray Beam Collimation

The X-ray beam collimation has both direct and indirect effect on patient radiation dose. The direct effect of beam collimation on patient radiation dose is differing between single detector scanners compared to multi detector scanners. For a single detector scanner exposure using a single wide collimator with all other parameters kept constant, allows more X-ray photons to be detected and causes more scatter. In contrast, less photon transmitted with thinner collimation results in less photons detected and hence increased statistical image noise. Thinner collimations typically result in a greater degree of overlap and higher CTDI values due to the over beaming factor. In multi detector scanners, the effect of differences in beam collimation is significant for narrower beam collimation, which manifests a higher degree of overlap.

e). Object Diameter

If all parameters remain constant, a smaller diameter object always absorbs a higher amount of radiation dose than a larger object. This is because tissues are being exposed with both entrance radiation and exit radiation as the source move around the patient. The smaller the patient, the higher the exit dose as the beam has been attenuated by less tissue and the dose distribution across the patient is much more uniform at all locations. For the larger patient, the exit radiation is much less due to its attenuation through more tissue.

2.1.6 CT number or Hounsfield units [10]

After CT reconstruction, each pixel in the image is represented by a high precision floating point number that is useful for computation but less useful for display. Most computer display hardware makes use of integer images. Consequently, after CT reconstruction, but before storing and displaying, CT images are normalized and truncated to integer values. The number CT(*x*,*y*) in each pixel, (*x*,*y*), of the image is converted using the equation 2.12:

$$CT\ (x,y) = 1{,}000\ x\frac{\mu\ (x,y)-\mu_{water}}{\mu_{water}} \qquad (2.12)$$

where μ *(x,y)* is the floating point number of the *(x,y)* pixel before conversion, μ_{water} is the attenuation coefficient of water, and CT *(x,y)* is the CT number (Hounsfield unit) that ends up in the final clinical CT image. The value of μ_{water} is about 0.195 for the x-ray beam energies typically used in CT scanning. This normalization results in CT numbers ranging from about - 1,000 to + 3,000, where - 1,000 corresponds to air, soft tissues range from - 300 to - 100, water is 0, and dense bone and areas filled with contrast agent range up to + 3,000.

CT images are produced with a highly filtered, high-kV x-ray beam, with an average energy of about 75 keV. At this energy in muscle tissue, about 91% of x-ray interactions are Compton scatter. For fat and bone, Compton scattering interactions are 94% and 74%, respectively. Therefore, CT numbers and hence CT images derive their contrast mainly from the physical properties of tissue that influence Compton scatter. Density (g/cm^3) is a very important discriminating property of tissue (especially in lung tissue, bone, and fat), and the linear attenuation coefficient, μ, tracks linearly with density. Other than physical density, the Compton scatter cross section depends on the electron density (ρ_e) in tissue: ρ_e = NZ/A, where N is Avogadro's number (6.023×10^{23}, a constant), Z is the atomic number, and A is the atomic mass of the tissue. The main constituents of soft tissue are hydrogen (Z = 1, A = 1), carbon (Z = 6, A = 12), nitrogen (Z =7, A = 14), and oxygen (Z = 8, A = 16). Carbon, nitrogen, and oxygen all have the same Z/A ratio of 0.5, so their electron densities are the same. Because the Z/A ratio for hydrogen is 1.0, the relative abundance of hydrogen in a tissue has some influence on CT number. Hydrogenous tissue such as fat is well visualized on CT. Nevertheless, density (g/cm^3) plays the dominant role in forming contrast in medical CT.

CT numbers are quantitative, and this property leads to more accurate diagnosis in some clinical settings. For example, pulmonary nodules that are calcified are typically benign, and the amount of calcification can be determined from the CT image based on the mean CT number of the nodule. Measuring the CT number of a single pulmonary nodule is therefore common practice, and it is an important part of the diagnostic work-up. CT scanners measure bone density with good accuracy, and when phantoms are placed in the field along with the patient, quantitative CT techniques can be used to estimate bone density, which is useful in assessing fracture risk. CT is also quantitative in terms of linear dimensions, and therefore it can be used to accurately assess tumor volume or lesion diameter.

2.1.7 Noise [10]

In a CT scanner, if one image a uniform material (e.g., a water bath) and looks at the CT-numbers for a localized region, one would find that the CT-numbers are not all the same, but that they vary around some average or mean value. This variation is called the noise of the system. Noise is a very important measure of CT scanner performance since the naturally occurring difference in attenuation coefficient between normal and pathological tissues is small. Noise of a CT scanner can be measured by scanning a uniform water phantom. This should be done for all potential modes (subject size, kVp, and scan diameters/pixel widths) of clinical use. The noise should be indicated by the standard deviation (figure 2.11). Noise should be examined for both central and peripheral regions of a scan.

Scan to scan precision for a given topographic section (detector system) can be obtained by the determination of the standard error (deviation of the mean) from 15 consecutive scans of a water phantom. Precision between topographic slices (detector systems) of the same scan can be made by comparison of the means and standard deviation for the same matrix area for both slices from a single scan of water.

2	-2	-3	0	-6	-6	1	0
4	1	2	5	-1	1	5	3
2	-1	0	5	0	0	2	1
-1	-1	-2	0	0	1	0	0
1	1	-2	-1	1	-1	-4	-2
-2	2	-1	0	1	-1	-3	0
6	-3	2	1	-4	3	1	4
3	4	2	-4	-3	-1	-2	-5

(A)

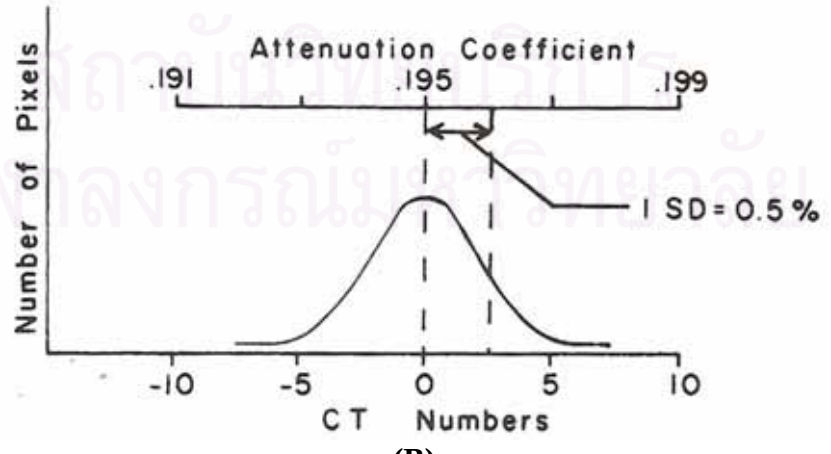

(B)

Figure 2.11 (A.) Typical CT number in an image of a volume of water.
(B.) The Spread of values (Standard Deviation).

Noise in CT image is a variation in CT number values from pixel to pixel and exists even when all pixels are associated with the same material.

2.1.7.1Effect on Visibility

Figure 2.12 shows three isometric images; each one has similar contrast, but the amount of noise increases toward the right of the figure. Noise interjects a random or stochastic component into the image (or other measurement), and there are several different sources of noise in an image. There are different concepts pertaining to noise that are useful as background to this topic. Noise adds or subtracts to a measurement value such that the recorded measurement differs from the actual value. Most experimental systems have some amount of noise, and some have a great deal of noise. If we measure some value repeatedly, for instance the number of counts emitted from a weak radioactive source, we can compute the average count rate (decays/second), and there are ways to calculate the standard deviation as well. In this example, multiple measurements are made to try to improve the accuracy of the mean value because there are large fluctuations in each individual measurement. These fluctuations about the mean are stochastic in nature, and the determination of the standard deviation (σ) relates to the precision of the measurement.

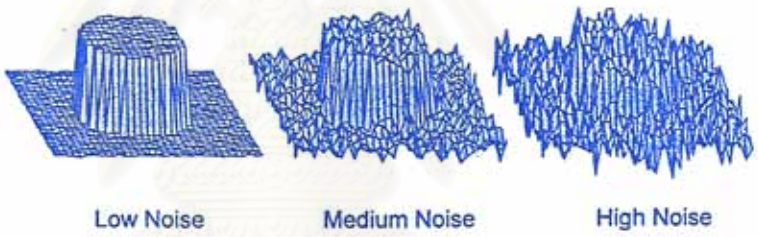

Figure 2.12 Isometric display for the concept of noise.

Many types of data have a normal distribution. The normal distribution is also known as the Gaussian distribution, and its mathematical expression is

$$G(x) = ke^{-\frac{1}{2}\left(\frac{\bar{x}-x}{\sigma}\right)^2} \qquad (2.13)$$

Notice that these two parameters, $\overline{X}$ and σ, describe the shape of the Gaussian distribution. The parameter x in Equation 2.13 is called the dependent variable, the value of k is just a constant, used to normalize the height of the curve.

2.1.7.2 Factors affecting Noise

Several factors associated with a CT procedure affect the amount of image noise, and they can be changed, to some degree, by the operator. As each factor is changed to reduce noise, it either adversely affects another aspect of image quality increases patient exposure. The amount of noise is inversely related to the total amount of radiation absorbed in each voxel; changing either the dimension of a voxel or the exposure produced by the x-ray beam alters the noise level.

a). Pixel Size

Noise can be decreased by increasing the dimensions of the pixel (voxel), but, as we have seen, this increases image blurring and reduces visibility of detail. This is one of the important compromises that must be made in selecting imaging factors.

b). Slice thickness

Since slice thickness forms one dimension of the voxel, it affects image noise. Thin slice, which produce better detail and fewer partial-volume artifacts, produce higher noise level. Again, a compromise must be made in selecting imaging factors.

c). Radiation Exposure

The amount of radiation used to create a CT image can usually be varied by changing either the mA or the scanning time. Changing either produces a proportional change in patient dose and the radiation absorbed in individual voxels. Image noise can be decreased by increasing the quantity of radiation used (mAs), but the radiation dose absorbed by the tissue will also increase.

2.1.8 Agar, Tissue Equivalent Material

The agar cone phantom as the tissue equivalent phantom is used in this study. Agar is widely used due to the commercially available and low price. Agar is insoluble in cold water but dissolve in boil water. It will be in solid form after cool down for 2-4 hours. It has been reported that the agar is suitable to simulate tissue as homogeneous phantom [20, 21, 22].

Figure 2.13 Agar

2.2 Literature review

Siegel MJ, et al. [23] evaluated the effects of varying tube current and kilo voltage on radiation dose, image noise and image contrast with different phantom size and shapes. Four round Lucite phantoms 8- 32 cm diameters were scanned with multi-detector row computed tomography (CT) using 80-120 kVp. Radiation dose was based on CT dose index, image noise, and iodine contrast and measured with contrast and variable tube currents that were appropriate for each tube voltage. Radiation dose, image noise and contrast were compared in round and oval 24 cm phantom. For various combinations of technical factors, phantom size and shapes, percentage differences were calculated for radiation dose, image noise and contrast. Reduced tube voltage for phantom diameter of contrast material-enhanced CT reduces radiation dose and maintains image contrast. Image noise increases, but the effect is minimal in smaller phantoms.

Brisse HJ, et al. [6] studied an AEC system on pediatric phantoms by studying the impact of phantom transmission and acquisition parameters on tube current modulation, on the absorbed dose and image quality. The study was performed with six cylindrical (polymethylmethacrylate) PMMA phantoms of variable diameters 10–32 cm and 5 years of age equivalent pediatric anthropomorphic phantom. After a single scan projection radiograph SPR, helical acquisitions were performed and images were reconstructed with a standard convolution kernel. Tube current modulation was studied with variable SPR settings (tube angle, mA, kVp) and helical parameters (6–20 HU noise indices, 80–140 kVp tube potential, 0.8–4.0 s. tube rotation time, 5–20 mm x-ray beam thickness, 0.75–1.5 pitch, 1.25–10 mm image thickness, variable acquisition, and reconstruction fields of view). CT dose indices ($CTDI_{vol}$) were measured, and the image quality criterion used was the standard deviation of the CT number measured in reconstructed images of PMMA material. The measured absorbed doses in each specific phantom can actually be fitted to an exponential curve leading to an observed linear attenuation factor very close to expected value. Observed tube current levels were compared to the expected values from Brooks and Di Chiro‘s [R.A. Brooks and G.D. Chiro, Med. Phys. 3, 237–240 (1976)] model and calculated values. This study demonstrates that this AEC system accurately modulates the tube current according to phantom size, but a PMMA phantom led to a discontinuity measurement artifact at phantom junctions and minimal variation of the noise.

Muramatsu Y, et al [24] studied the performance of the latest CT-AEC of each manufacturer with the aim of establishing a standard CT-AEC performance evaluation method. The design of the phantoms was based upon the operation characteristics of different CT-AEC. A cone, an ellipse, a variable-shaped ellipse, stepped phantom, and their analysis software were devised and carried out the field test. The targets were Light Speed VCT64 with Auto mA (GE), Aquilion 64M with Real-EC (Toshiba), Sensation 64 with CARE Dose 4D (Siemens), and Bulliance 16P with Dose Right(Philips). Data was acquired while varying the typical abdominal CT (with CT-AEC) scanning conditions. The results reflect the basic concept and performance characteristics of the methods. Standardization of CT-AEC performance evaluation is possible using these phantoms.

CHAPTER III

RESEARCH METHODOLOGY

3.1 Research design

This study is an observational research.

3.2 Research design model

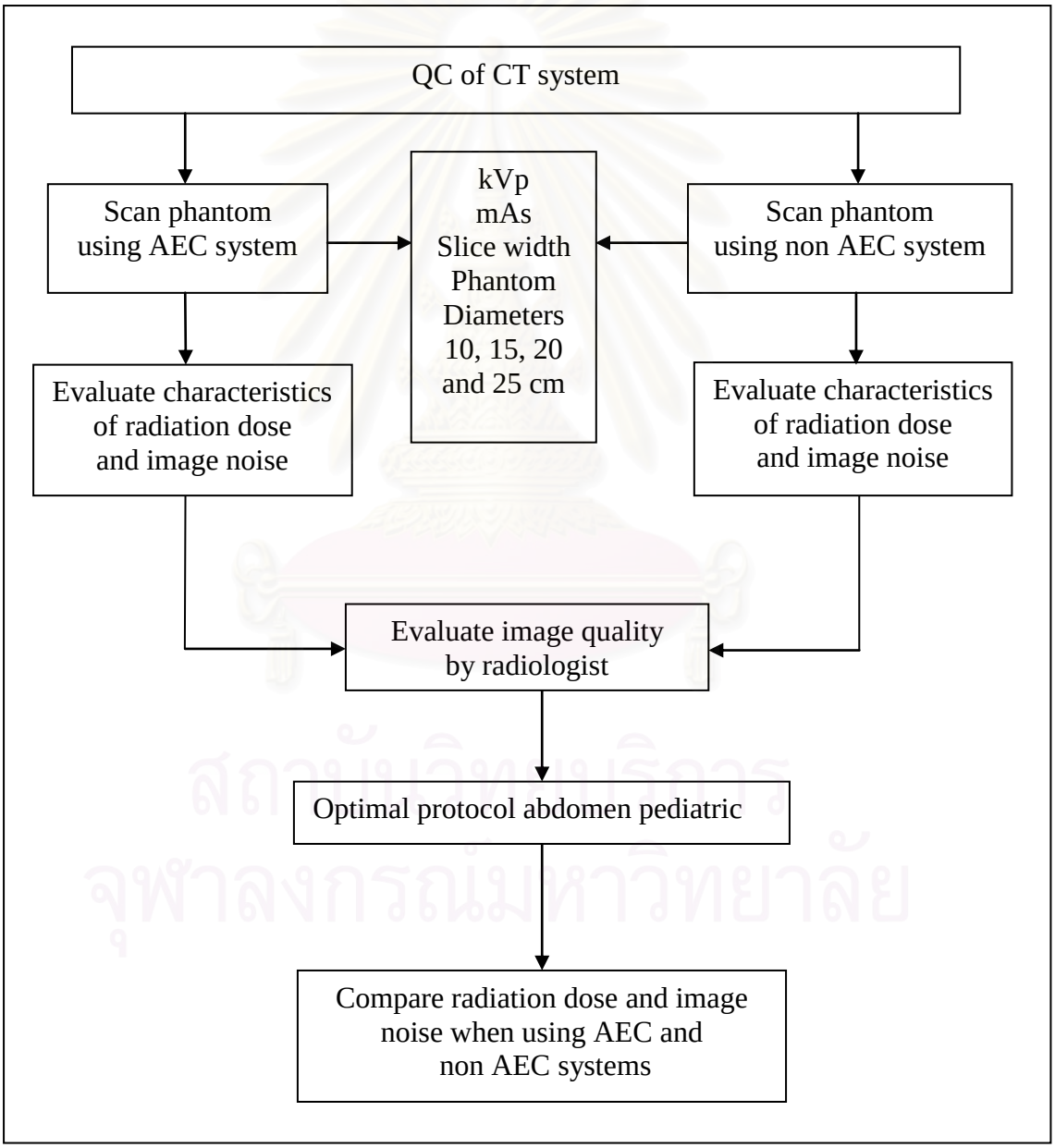

Figure 3.1 Research design model.

3.3 Conceptual framework

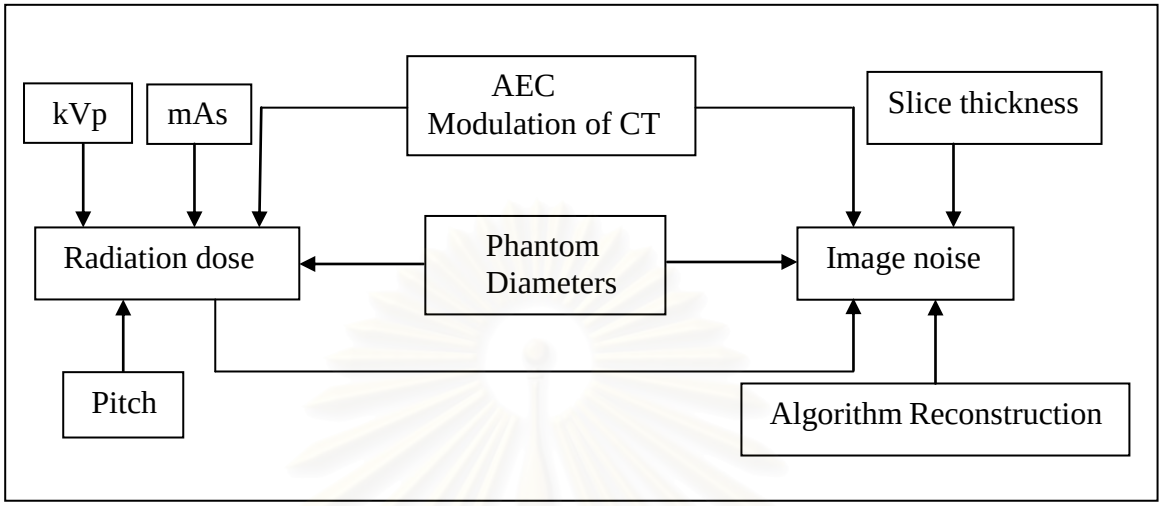

Figure 3.2 Conceptual frameworks.

3.4 Keywords

- Multi-Slice Computed Tomography (MSCT)
- Automatic Exposure Control (AEC)
- Image Quality
- Pediatric Phantom

3.5 Research Questions

3.5.1 Primary Question

What are the characteristics of AEC system for Siemens Sensation 16 MSCT using cone phantom? (pediatric study)

3.5.2 Secondary Question

What are the differences in radiation dose and image noise when using AEC system and non AEC system?

3.6 Materials

3.6.1 CT equipment Siemens Somatom Sensation 16 and Automatic exposure control (AEC) system installed in 2003. The Siemens Sensation 16 is the 7th generation multi slice helical CT scanner, featuring a 60 kW generator, 5.3 MHU x-ray tube and a fastest gantry rotation time of 0.42 seconds. In helical mode it is capable of imaging 16 slices per rotation, with slice widths of 16 x 1.5 mm and 16 x 0.75 mm, as well as smaller numbers of wider slices. It has 24 parallel rows of solid-state detectors, covering 24 mm in the z direction at the isocenter.

Figure 3.3 The computed tomography equipment.

3.6.2 Phantom

Two types of phantom were used for this study: cylindrical PMMA CT head phantom and one cone phantom filled with agar to simulate pediatric patient of different diameters.

3.6.2.1 Polymethylmethacrylate $[(C_5H_8O_2)_n$, PMMA] cylindrical CT head phantom with 16 cm diameter as shown in figure 3.4, was used to determine the radiation dose. Phantom length along the z-axis was 15 cm. Holes were drilled in the phantom, in which a pencil ionization chamber 100 mm: DCT 10-RS S/N1057 was placed.

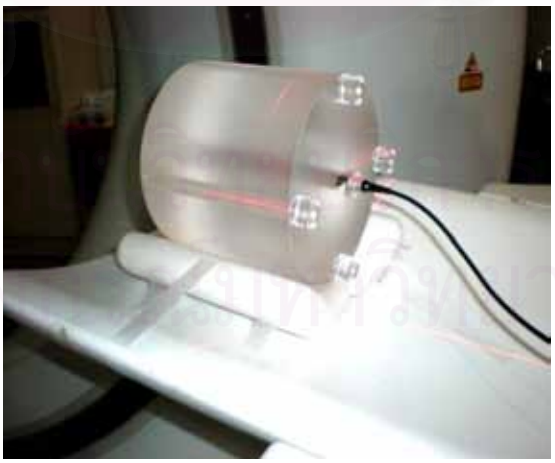

Figure 3.4 The Polymethylmethacrylate cylindrical phantom 16 cm.

3.6.2.2 Agar cone phantom simulate pediatric patient of various diameters was used to determine the dose and image noise and each diameters represent age groups following:

- 10 cm diameter represents 1 year (4 months-2 years 11 months)
- 15 cm diameter represents 5 years (3 years-7 years 11 months)
- 20 cm diameter represents 10years (8 years-14 year 11 months)
- 25 cm diameter represents >15 years-old

The agar cone phantom of 40 cm largest diameter and 40 cm length 0.3 cm thickness made of acrylic container with solid agar consisted of water and agar (500 ml: 8 g) inside the phantom as shown in figure 3.5.

Figure 3.5 The agar cone phantom simulate pediatric patient.

3.6.3 Pencil ionization chamber 100 mm length: Manufacturer RTI Solidose Model, DCT 10-RS S/N1057

The 10 cm CT pencil ionization chamber is shown in Fig 3.6. It has 4.9 cm^3 active volumes, 100 mm total active length, 8.0 mm inner diameter of out electrode, and 1.0 mm diameter of inner electrode.

Figure 3.6 Pencil ionization chamber

3.6.4 Dosimeter

Electrometer RTI Electronic AB type SOLIDOSE 400 electrometer S/N 4103 as shown in Fig 3.7, connecting with pencil ionization chamber. It has the leakage within 4×10^{-15} Ampere, for 80 – 150 kV radiation quality, and the calibration factor $N_{D,K}$ equal to 24.2 mGy.cm/nC (120 kV/HWD 4.05 mm Al).

Figure 3.7 Electrometer

3.6.5 Quality Control equipment

3.6.5.1 Catphan® 500

The Catphan ®500 is shown in Fig 3.8 and designed to address the specific testing needs associated with spiral CT scanning. It is used for the image quality evaluation.

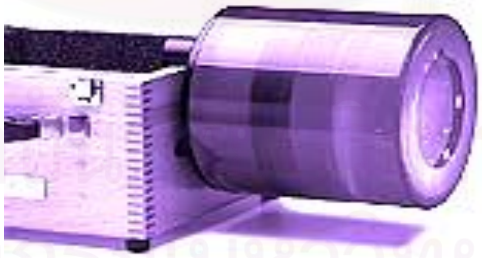

Figure 3.8 Catphan® 500

3.6.5.2 KODAK X-OMAT V film

Kodak X-OMAT V film size 10x12 in is shown in Fig 3.9, will be used for verification imaging. These are only available in Ready Pack packaging and can also be used for quality control procedures such as slice thickness, slice width, laser and x-ray beams congruence test.

Figure 3.9 KODAK X-OMAT V film

3.7 Methods

3.7.1 Perform the quality control of MSCT scanner.

3.7.1.1 Following standard of AAPM No. 39 [25]:

- Scan localization light accuracy
- Alignment of table to gantry
- Table increments accuracy
- Slice increment accuracy
- Radiation profile
- Gantry tilt
- Position dependence and S/N ratio of CT numbers
- Reproducibility of CT numbers
- Linearity of CT numbers
- High contrast resolution
- Low contrast resolution
- mAs linearity

3.7.2 Verification of exposure dose

In order to verify the accuracy of the exposure dose, the followings will be studied and compared the difference between dose shown on CT monitor the dose meter monitors and ImPACT values

- $CTDI_{100}$,
- $CTDI_{w}$,
- $CTDI_{vol}$

3.7.3 Scan agar cone phantom using AEC system (CARE Dose 4D) quality reference mAs = 55 (Protocol abdomen pediatric) and non AEC with the following parameters kVp at 80, 100 and 120 and mAs at 50, 70, 90 and 110. Slice thickness 5 mm, collimation 16x0.75 mm and pitch 1 were selected for the phantom diameters at 10, 15, 20 and 25 cm.

3.7.3.1 Record $CTDI_{vol}$ from CT monitor.

3.7.3.2 Measure image noise for the circular ROI area of 2 cm^2 at center and periphery of image (5 points), 3 times, record the standard deviations (SD) and average image noise.

3.7.4 Evaluate the characteristics of AEC and non AEC systems on radiation dose ($CTDI_{vol}$) and image noise on the agar cone phantom of different diameters.

3.7.5 Evaluation Image Quality by radiologist

Grading image noise of AEC and non AEC systems in pediatric phantom image:

Level of grading:

1 = not acceptable
2 = acceptable
3 = good
4 = very good

3.7.6 Compare the radiation dose ($CTDI_{vol}$) and image noise when using AEC and non AEC systems in agar cone phantom.

3.8 Sample size

Due to the phantom study and parameters:

AEC system

Agar cone phantom diameters = 10, 15, 20 and 25 cm
kVp = 80, 100 and 120
Sample size = 3x4 = 12

Non AEC system

Agar cone phantom diameters = 10, 15, 20 and 25 cm
kVp = 80, 100 and 120
mAs = 50, 70, 90 and 120
Sample size = 3x4x4 = 48

Total Sample size = 12 + 48 = 60

3.9 Statistical Analysis

The radiation dose and noise are continuous data.

-Descriptive statistics
-Mean
-Standard deviation (SD)
- Compare two groups
- Paired t-test

3.10 Data Presentation

The tables and graphs were presented.

3.11 Ethical Considerations

The Ethic Committee of Faculty of Medicine, Chulalongkorn University had approved the research proposal.

3.12 Expected benefits

3.12.1 Performance Characteristics of AEC system for Siemens Sensation 16 MSCT were obtained and implemented in pediatric study.

3.12.2 Factors affecting the radiation dose and image noise.

3.12.3 Optimal pediatric dose and image noise when using AEC system and non AEC system.

CHAPTER IV

RESULTS

4.1 Quality control of the MSCT (Appendix B)

4.2 Verification of exposure dose

4.2.1 $CTDI_{100}$ measured in air

The result of radiation dose measurement in air of head and body acquisition protocol was compared to ImPACT scan values. They were within ±10% error as shown in (table 4.1).

Table 4.1 $CTDI_{100}$ in air (head and body) measured at different kVp, 100 mA, 1sec, 1 pitch, 2 x 5 mm collimation.

kVp	$CTDI_{100}$ (Head) (mGy)	ImPACT (mGy)	% error	$CTDI_{100}$ (Body) (mGy)	ImPACT (mGy)	% error
80	8.36	9.1	-8.15	4.93	5.24	-5.9
100	14.94	-	-	9.95	-	-
120	20.47	21.8	-6.1	14.68	15.26	-3.78
140	28.89	-	-	21.85	21.63	1.03

4.2.2 $CTDI_{100}$ and $CTDI_w$ in phantom

4.2.2.1 $CTDI_{100}$ in head phantom

The result of radiation dose measurement in phantom of head and body was compared with ImPACT scan values (table 4.2).

Table 4.2 $CTDI_{100}$ at each position of CT head phantom at the different kVp, 100 mA, 1sec, 1 pitch, 2 x 5 mm collimation and kernel H30s.

kVp	$CTDI_{100}$ (mGy)									
	At Peripheral							At Center		
	Top	Bottom	Left	Right	Average	ImPACT	% error	center	ImPACT	% error
80	6.06	5.31	5.78	5.9	5.76	6.7	-14.05	4.76	5.5	-13.5
100	11.29	10.02	10.93	10.99	10.77	-	-	9.32	-	-
120	15.73	14.09	14.93	15.25	15.02	17.2	-12.65	13.35	15.4	-13.31
140	22.38	20.14	21.57	21.71	21.41	-	-	19.25	-	-

Table 4.3 $CTDI_w$ of CT head phantom at the different kVp, 100 mA, 1sec, 1 pitch, 2 x 5 mm collimation and kernel H30s.

kVp	80	100	120	140
$CTDI_w$(mGy)	5.43	10.29	14.47	20.69

4.2.2.2 $CTDI_{100}$ in body phantom

The result of radiation dose measurement in phantom of body was compared with ImPACT scan values (table 4.4).

Table 4.4 $CTDI_{100}$ at each position of CT body phantom at the different kVp, 100 mA, 1sec, 1 pitch, 2 x 5 mm collimation and kernel B30s.

	$CTDI_{100}$(mGy)									
kVp	Periphery							Center		
	Top	Bottom	Left	Right	Ave-rage	Im-PACT	% error	Center	Im-PACT	% error
80	2.32	1.8	2.14	2.16	2.09	2.6	-19.58	0.91	1.12	-19.2
100	4.66	3.88	4.51	4.62	4.39	-	-	2.15	-	-
120	7.09	5.79	6.84	6.93	6.6	8.16	-19.08	3.39	4.17	-18.75
140	10.77	9.1	10.25	10.37	10.08	-	-	5.26	6.19	-14.99

Table 4.5 $CTDI_w$ of CT body phantom at the different kVp, 100 mA, 1sec, 1 pitch, 2 x 5 mm collimation and kernel B30s.

kVp	80	100	120	140
$CTDI_w$(mGy)	1.7	3.64	5.53	8.48

4.2.3 $CTDI_{vol}$ of monitor and calculated $CTDI_w$

4.2.3.1 $CTDI_{vol}$ displayed on monitor for head phantom

The result of radiation dose measurement in head phantom, $CTDI_{vol}$ displayed on the monitor were compared to ImPACT scan values (table 4.6).

The percent errors among $CTDI_{vol}$ displayed on monitor and ImPACT values are less than 10, showing the acceptable values.

Table 4.6 $CTDI_{vol}$ of monitor and $CTDI_w$ using head techniques mAs 100, collimation 10 mm and pitch 1 and kernel H30s.

kVp	$CTDI_{vol}$ (mGy)				
	calculated	monitor	% error (calculated and monitor)	ImPACT	% error (ImPACT and monitor)
80	5.43	6.70	-19.03	6.30	-6.3%
100	10.29	11.20	-8.16	-	-
120	14.47	16.80	-13.89	16.60	-1.2%
140	20.70	22.90	-9.65	-	-

4.2.3.2 $CTDI_{vol}$ of monitor for body phantom

The result of radiation dose measurement in phantom of body was compared with ImPACT scan values (table 4.7).

The percent errors among $CTDI_{vol}$ displayed on monitor and ImPACT values are less than 10, showing the acceptable values.

Table 4.7 $CTDI_{vol}$ of monitor and $CTDI_w$ using body techniques mAs 100, collimation 10 mm and pitch 1 and kernel B30s.

kVp	$CTDI_{vol}$ (mGy)				
	calculated	monitor	% error (calculated and monitor)	ImPACT	% error (ImPACT and monitor)
80	1.70	2.10	-19.26	2.10	0%
100	3.64	4.00	-9.01	-	-
120	5.53	6.30	-12.20	6.83	7.76%
140	8.48	9.10	-6.87	-	-

4.3 AEC Characteristics on agar cone phantom.

4.3.1 The effect of variation on kVp and diameter on dose and noise

The data from AEC system when varying kVp was shown in table 4.8. The effective mAs modulated along diameters of a cone phantom resulting in variation of $CTDI_{vol}$ and noise.

Table 4.8 $CTDI_{vol}$ and noise for kVp of 80,100 and 120, AEC mode for the agar cone phantom of various diameters.

AEC									
	80 kVp			100 kVp			120 kVp		
Diameter (cm)	Eff. mAs	CTDI $_{vol}$ (mGy)	Noise (HU)	Eff. mAs	CTDI $_{vol}$ (mGy)	Noise (HU)	Eff. mAs	CTDI $_{vol}$ (mGy)	Noise (HU)
10	45	1.17	9.36±0.63	43	2.15	6.88±0.26	43	3.35	5.32±0.37
15	59	1.53	12.82±0.70	59	2.95	8.72±0.22	60	4.68	7.16±0.45
20	83	2.16	19.18±2.36	84	4.2	11.78±0.78	83	6.47	9.46±0.84
25	116	3.02	28.42±2.54	117	5.85	16.98±1.03	117	9.13	13.08±1.12

Automatic exposure control (AEC) activated has adjusted eff. mAs according to various diameters. Eff. mAs are modulated of similar values for various diameters and different kVp. The correlation between eff. mAs range 43-117 and diameters (figure 4.1) was R^2= 0.999.

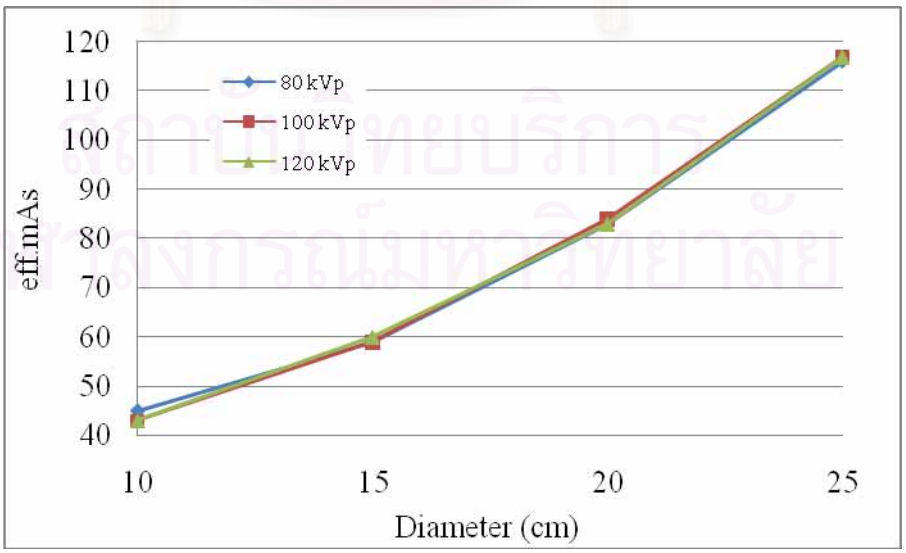

Figure 4.1 The relationship between eff. mAs and phantom diameter for kVp 80, 100 and 120 using AEC mode.

The AEC has automatically modulated the effective mAs resulting in $CTDI_{vol}$ increasing as the phantom diameter is increasing. As the tube voltage was increasing with increasing diameters, the $CTDI_{vol}$ was increasing as well (figure 4.2).

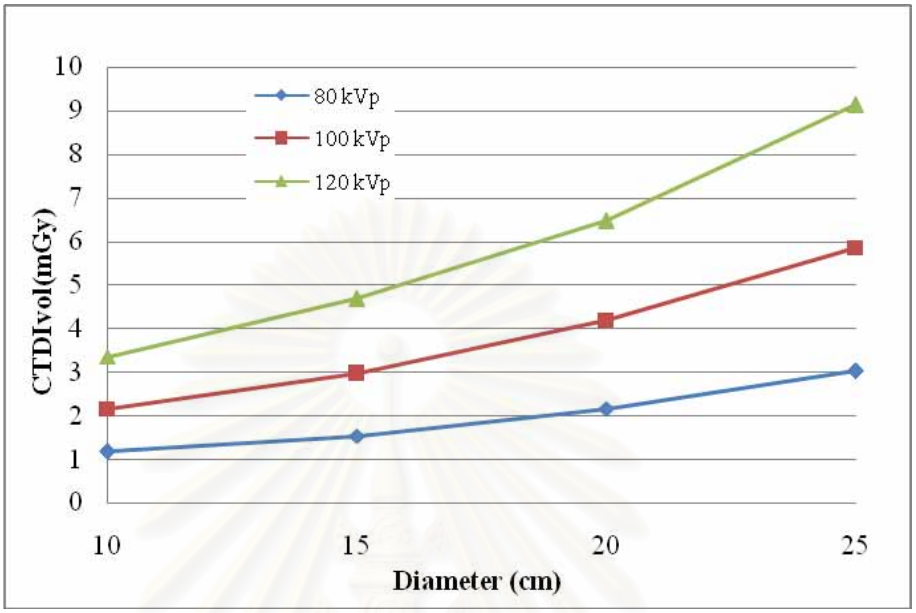

Figure 4.2 The relationship between $CTDI_{vol}$ and phantom diameters for kVp 80, 100 and 120 using AEC Mode.

At the contain tube voltage, the noise is increasing at increasing diameters. The increasing of tube voltage causes the decreasing of noise (figure 4.3).

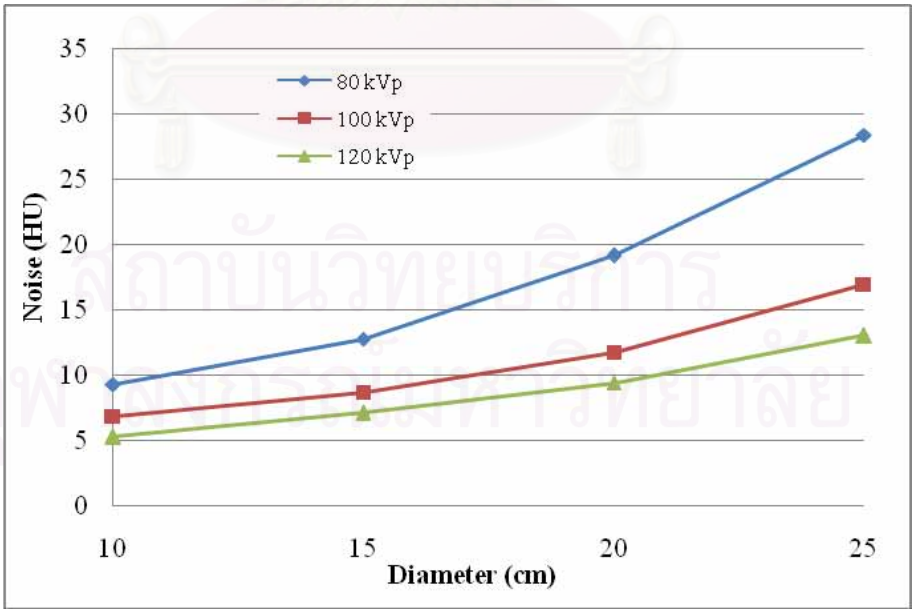

Figure 4.3 The relationship between noise and phantom diameters for kVp 80, 100 and 120

The relationship between dose and noise using AEC system in each kVp was shown in figure 4.4, the result shows that as kVp increases, the phantom diameter increases, $CTDI_{vol}$ increases, the noise also increases. At a certain phantom diameter, as kVp increases, the noise decreased.

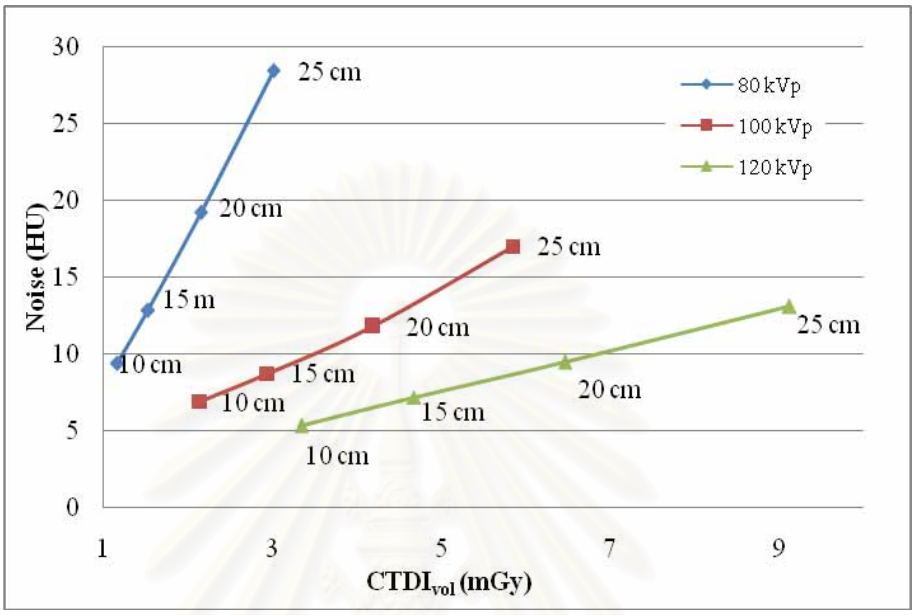

Figure 4.4 The relationship between the noise (HU) and $CTDI_{vol}$ (mGy) in each kVp and phantom diameter using AEC mode activated.

4.4 Non AEC Characteristics on agar cone phantom

The results from non AEC system using constant eff. mAs and varying kVp is shown in table 4.9. The results were $CTDI_{vol}$ increasing and noise decreasing at increasing phantom diameter and eff. mAs in each kVp.

Table 4.9 $CTDI_{vol}$ and noise for kVp at 80,100 and 120, and eff. mAs at 50, 70, 90, and 110, using non AEC mode for a cone phantom of various diameters.

Non AEC Characteristics							
Diameter (cm)	Eff. mAs	80 kVp		100 kVp		120 kVp	
		$CTDI_{vol}$ (mGy)	Noise (HU)	$CTDI_{vol}$ (mGy)	Noise (HU)	$CTDI_{vol}$ (mGy)	Noise (HU)
10	50	1.3	7.84±0.35	2.5	5.84±0.39	3.9	4.6±0.24
10	70	1.82	7.38±0.56	3.5	4.88±0.19	5.46	4.22±0.19
10	90	2.34	6.22±0.39	4.5	4.56±0.22	7.02	3.7±0.17
10	110	2.86	5.68±0.29	5.5	4.00±0.2	8.58	3.46±0.27
15	50	1.3	12.98±1.4	2.5	8.82±0.42	3.9	7.06±0.30
15	70	1.82	11.42±0.77	3.5	7.8±0.12	5.46	6.14±0.36
15	90	2.34	10.36±0.70	4.5	6.5±0.17	7.02	5.4±0.45
15	110	2.86	8.88±0.51	5.5	6.1±0.46	8.58	5.08±0.43
20	50	1.3	23.14±1.29	2.5	14.16±0.90	3.9	11.06±1.36
20	70	1.82	19.96±1.69	3.5	12.56±0.40	5.46	9.9±1.39
20	90	2.34	15.7±2.11	4.5	10.98±1.37	7.02	8.76±0.91
20	110	2.86	15.28±1.41	5.5	10.1±1.07	8.58	7.76±0.84
25	50	1.3	41.68±5.18	2.5	24.4±2.55	3.9	18.76±1.75
25	70	1.82	34.28±3.74	3.5	20.96±1.70	5.46	16.58±1.88
25	90	2.34	31.26±2.17	4.5	18.3±1.56	7.02	14.44±1.76
25	110	2.86	28.58±3.47	5.5	16.36±1.67	8.58	12.56±1.11

The results of non AEC system with a constant kVp at 80 and varying diameters and eff. mAs show the increases in noise at increasing diameters especially larger diameter as shown in figure 4.5. With the increasing eff. mAs the noise decreases very little at 10 cm diameter but larger at 25 cm diameter.

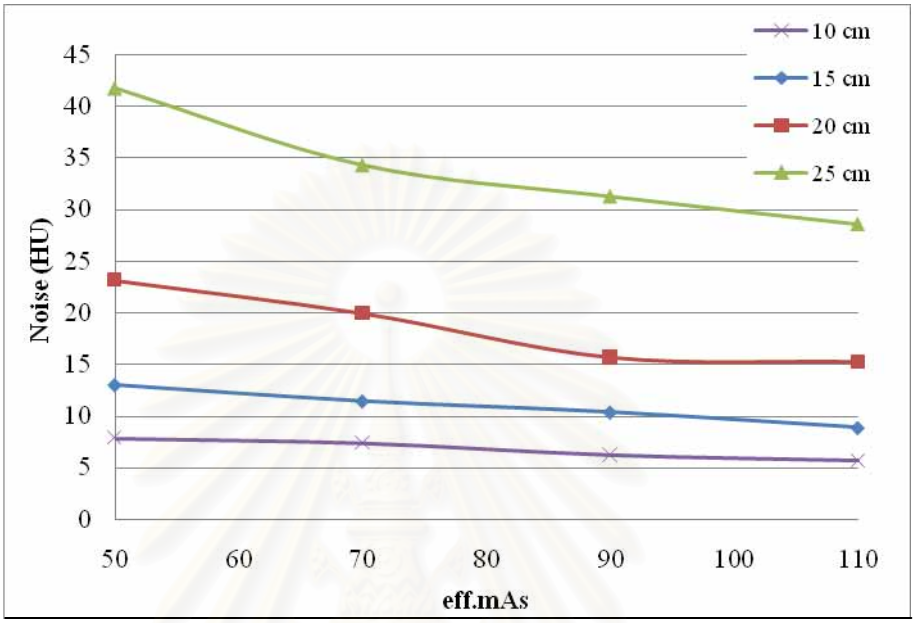

Figure 4.5 Noise and eff. mAs in each phantom diameters at 80 kVp using non AEC system.

With varying eff. mAs at phantom diameters of 10 cm in each kVp, the $CTDI_{vol}$ increases as shown figure 4.6.

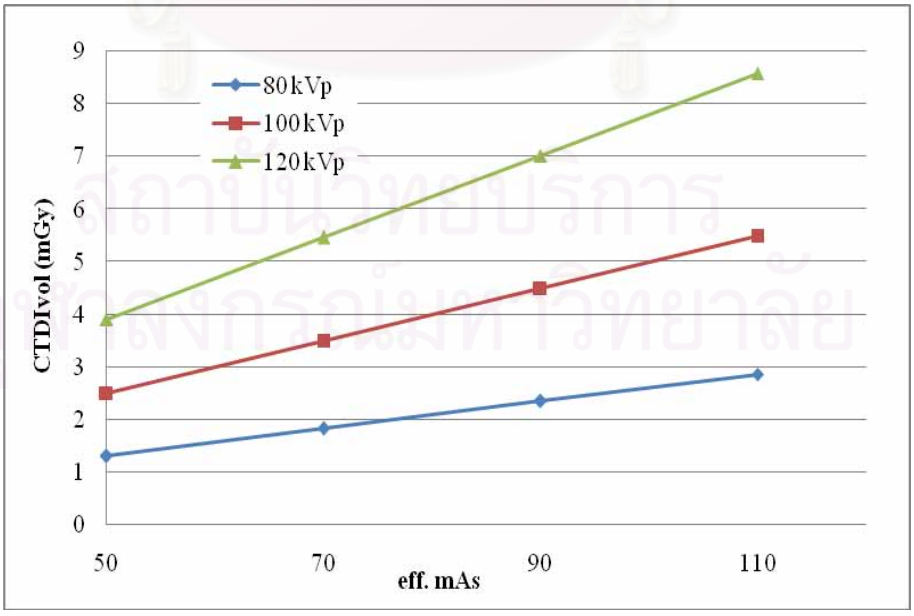

Figure 4.6 $CTDI_{vol}$ and eff. mAs at diameter 10 cm in each kVp using non AEC system.

When the eff. mAs is fixed at 70 vary kVp, $CTDI_{vol}$ constant at each diameter. For the 10, 15, 20 and 25 cm of cone phantom diameter, $CTDI_{vol}$ increased as kVp increased as shown in figure 4.7.

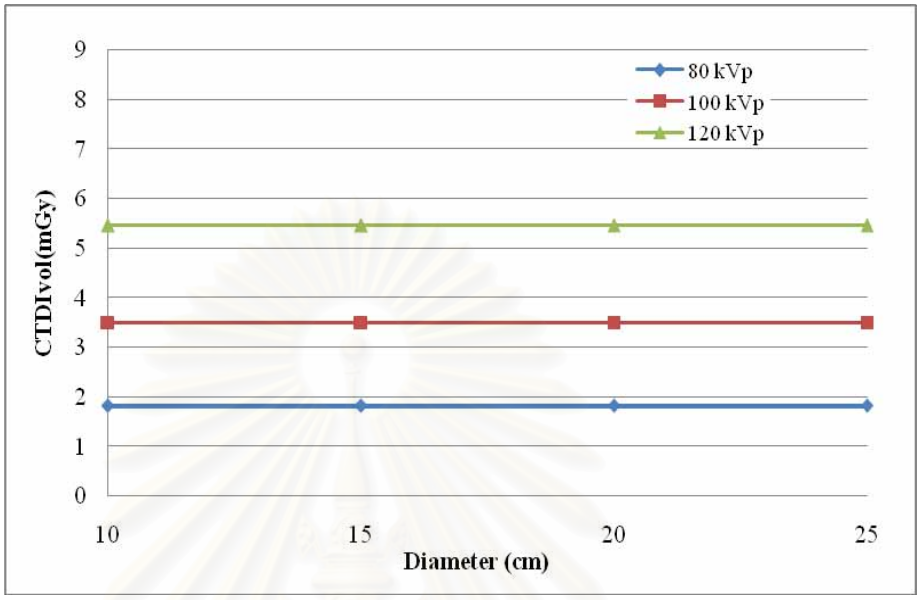

Figure 4.7 $CTDI_{vol}$ and phantom diameter in each kVp at eff. mAs 70 using non AEC system.

At a constant eff. mAs at 70, vary kVp, the noise increased with increasing phantom diameter. The increasing of tube voltage causes the decreasing of noise (4.22- 34.28 HU) (figure 4.8). The noise is increasing when the phantom diameter is increasing from 10-25 cm. The noise is reducing when kVp is increasing from 80 to 120.

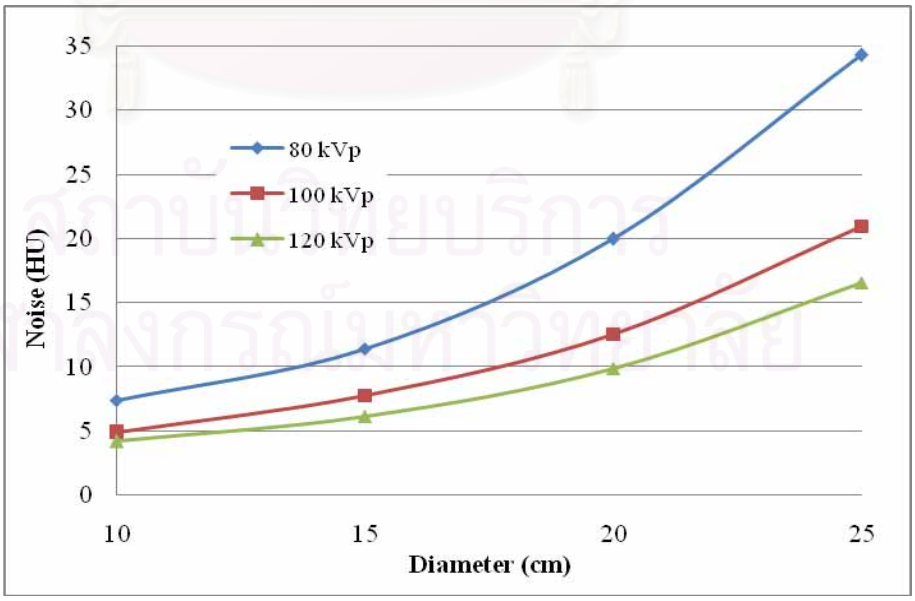

Figure 4.8 Noise and phantom diameter in each kVp at eff. mAs 70 using non AEC system.

4.5 AEC and non AEC activated.

4.5.1 $CTDI_{vol}$ and noise versus eff. mAs

The linear relationship exists between eff. mAs and $CTDI_{vol}$. $CTDI_{vol}$ increases as the increasing of the eff. mAs (figure 4.9 a). When the phantom diameter increases, the noise was increasing at the same kVp.(figure 4.9 b) At the constant phantom diameter, the increasing eff. mAs resulted in reducing noise. The image noise is inversely proportional to the square root of dose (eff. mAs) (figure 4.10 b).

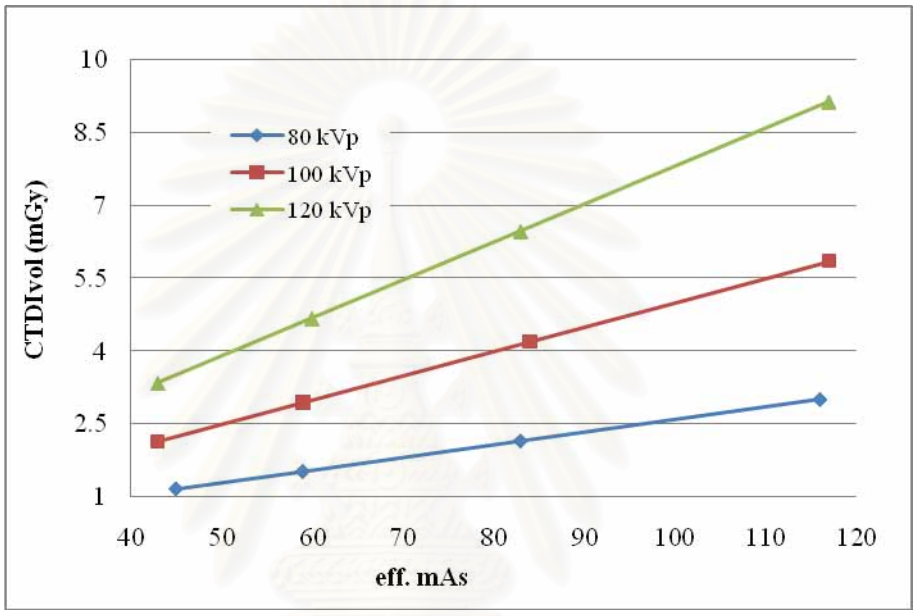

a)

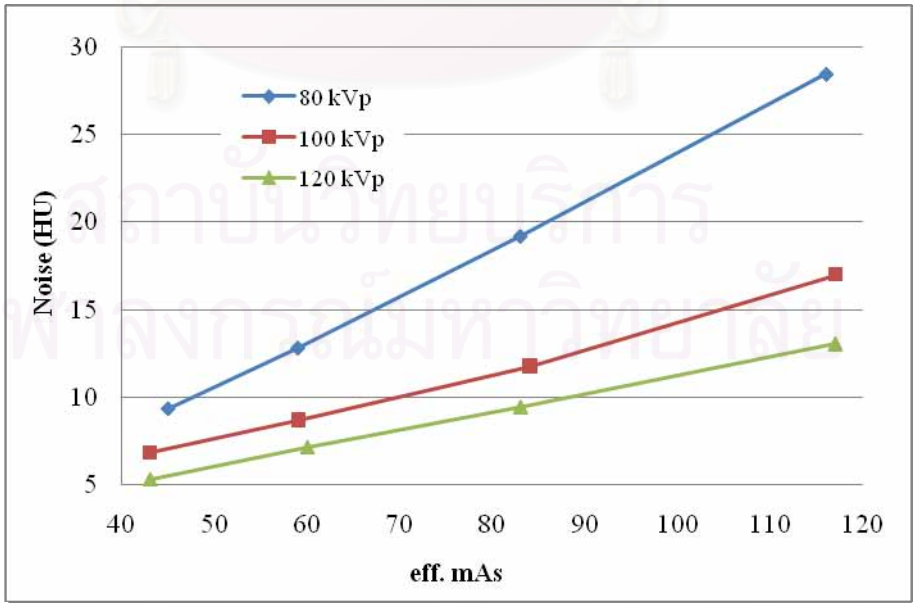

b)

Figure 4.9 $CTDI_{vol}$ and noise versus eff. mAs at each kVp for AEC mode.

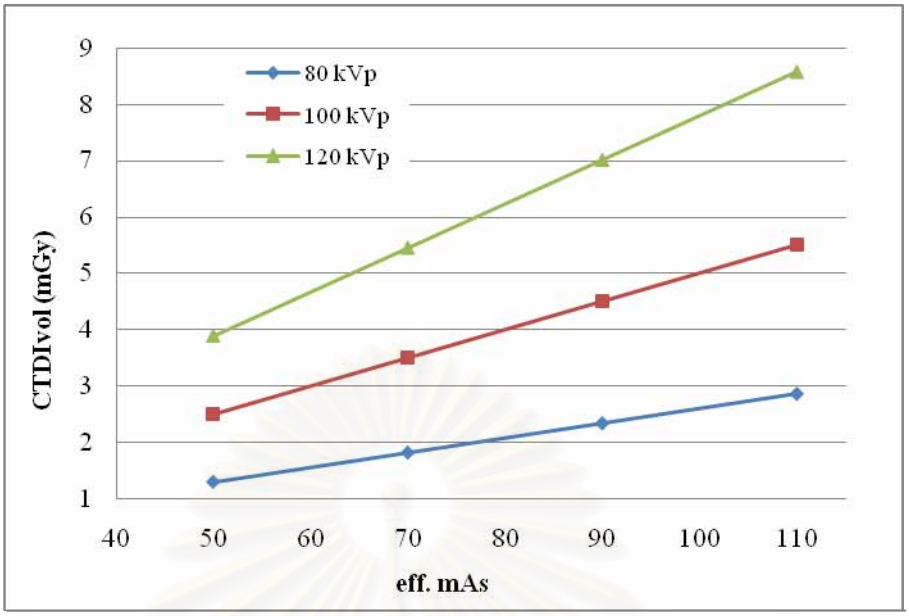

a)

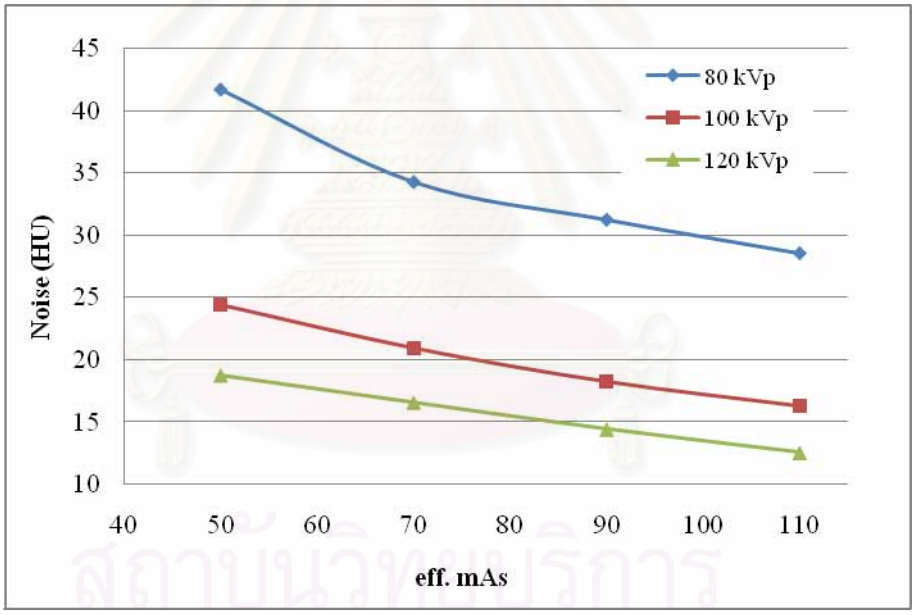

b)

Figure 4.10 $CTDI_{vol}$ and noise versus eff. mAs at 25 cm in each kVp for non AEC.

4.5.2 Correlation between dose and noise

The results show that noise decreased while $CTDI_{vol}$ increased. The correlations between noise and dose were exponential (figure 4.11 a and b). Image noise is inverse proportional to the square root of dose.

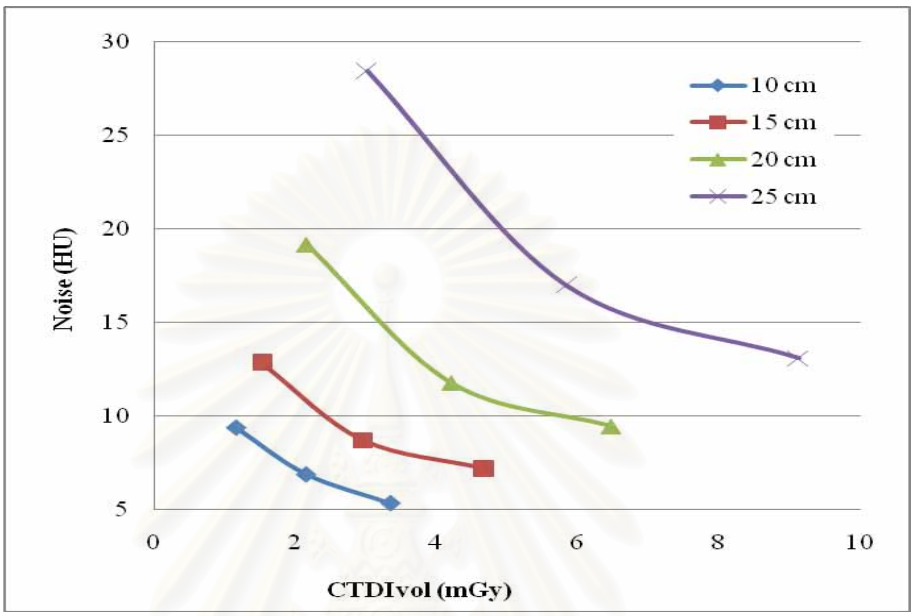

a)

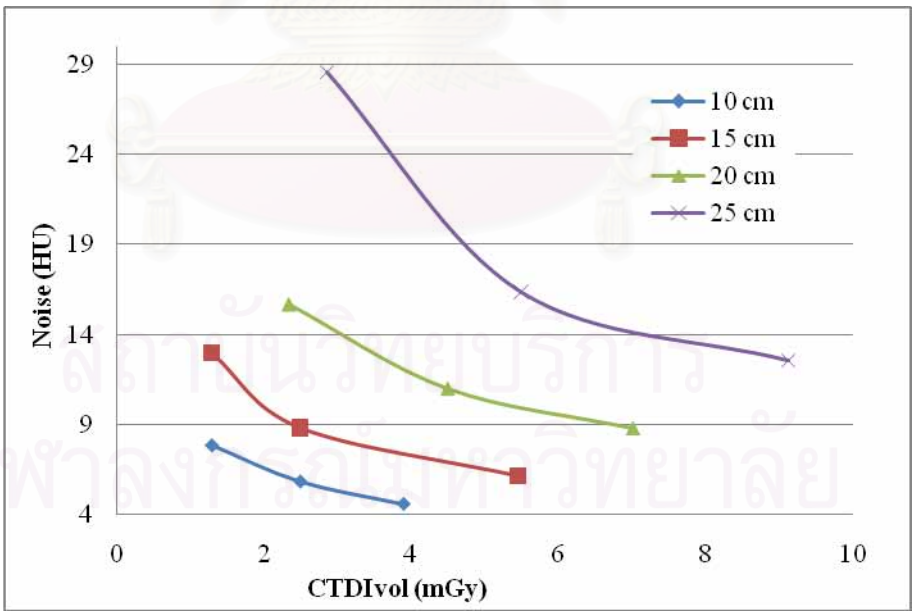

b)

Figure 4.11 Noise versus $CTDI_{vol}$ at phantom of various diameters in each kVp and at 110 eff. mAs for AEC (a) and non AEC (b) activated.

4.6 Evaluation of the image quality

The image quality scored by a radiologist when AEC and non AEC were used with a cone phantom as shown in table 4.10.

Table 4.10 Scoring criteria

Score	Overall quality
1	Not acceptable
2	Acceptable
3	Good
4	Very good

Total 60 images on conical phantom were scored for image quality. Among 60, there were 12 with AEC and 48 with non AEC.

The result on score 1, the image quality not acceptable of 9 images from 60 (15%) is shown in table 4.11 with exposure techniques, $CTDI_{vol}$ and noise.

Table 4.11 The image quality with score 1 of 9 images, AEC 2/9 (22%) and non AEC 7/9 (78%).

Diameter (cm)	Technique	$CTDI_{vol}$ (mGy)	Noise (HU)
20	80 kVp/70 mAs	1.82	19.96
20	80 kVp/50 mAs	1.3	23.14
20	80 kVp/AEC	2.16	19.18
25	80 kVp/90 mAs	2.34	31.26
25	80 kVp/110 mAs	2.86	28.58
25	80 kVp/50 mAs	1.3	41.68
25	80 kVp/70 mAs	1.82	34.28
25	80 kVp/AEC	3.02	28.42
25	100 kVp/50 mAs	2.5	24.4
Mean		2.12(1.3-3.02)	27.88(19.18-41.68)

Table 4.12 The image quality with score 2 of 25 images, AEC 7/25 (28%) and non AEC 18/25(72%).

Diameter (cm)	Technique	$CTDI_{vol}$ (mGy)	Noise (HU)
10	80 kVp/AEC	1.17	9.36
10	80 kVp/50 mAs	1.3	7.84
10	100 kVp/AEC	2.15	6.88
10	100 kVp/50 mAs	2.5	5.84
10	80 kVp/70 mAs	1.82	7.38
15	80 kVp/50 mAs	1.3	12.98
15	80 kVp/70 mAs	1.82	11.42
15	80 kVp/90 mAs	2.34	10.36
15	80 kVp/110 mAs	2.86	8.88
15	100 kVp/AEC	2.95	8.72
15	100 kVp/50 mAs	2.5	8.82
15	120 kVp/AEC	4.68	7.16
15	80 kVp/AEC	1.53	12.82
20	80 kVp/90 mAs	2.34	15.7
20	80 kVp/110 mAs	2.86	15.28
20	100 kVp/AEC	4.2	11.78
20	100 kVp/50 mAs	2.5	14.16
20	100 kVp/70 mAs	3.5	12.56
20	100 kVp/90 mAs	4.5	10.98
20	100 kVp/110 mAs	5.5	10.1
25	100 kVp/AEC	5.85	16.98
25	100 kVp/70 mAs	3.5	20.96
25	100 kVp/90 mAs	4.5	18.3
25	120 kVp/50 mAs	3.9	18.76
25	120 kVp/70 mAs	5.46	16.58
Mean		3.10 (1.17-5.85)	12.02 (5.84-20.96)

Table 4.13 The image quality with score 3 of 19 images, AEC 3/19 (16%) and non AEC 16/19 (84%).

Diameter (cm)	Technique	$CTDI_{vol}$ (mGy)	Noise (HU)
10	80 kVp/90 mAs	2.34	6.22
10	80 kVp/110 mAs	2.86	5.68
10	100 kVp/70 mAs	3.5	4.88
10	120 kVp/AEC	3.35	5.32
10	120 kVp/50 mAs	3.9	4.6
10	100 kVp/90 mAs	4.5	4.56
15	100 kVp/70 mAs	3.5	7.8
15	100 kVp/90 mAs	4.5	6.5
15	120 kVp/50 mAs	3.9	7.06
15	120 kVp/70 mAs	5.46	6.14
15	120 kVp/90 mAs	7.02	5.4
20	120 kVp/AEC	6.47	9.46
20	120 kVp/50 mAs	3.9	11.06
20	120 kVp/70 mAs	5.46	9.9
20	120 kVp/90 mAs	7.02	8.76
25	100 kVp/110 mAs	5.5	16.36
25	120 kVp/AEC	9.13	13.08
25	120 kVp/90 mAs	7.02	14.44
25	120 kVp/110 mAs	8.58	12.56
Mean		5.15(2.34-8.58)	8.41 (4.6-16.36)

Table 4.14 The image quality with score 4 of 7 images, AEC 0/7 (0%) and non AEC 7/7 (100%).

Diameter (cm)	Technique	$CTDI_{vol}$ (mGy)	Noise (HU)
10	100 kVp/110 mAs	5.5	4
10	120 kVp/70 mAs	5.46	4.22
10	120 kVp/90 mAs	7.02	3.7
10	120 kVp/110 mAs	8.58	3.46
15	100 kVp/110 mAs	5.5	6.1
15	120 kVp/110 mAs	8.58	5.08
20	120 kVp/110 mAs	8.58	7.76
Mean		7.03 (5.46-8.58)	4.90 (3.46-7.76)

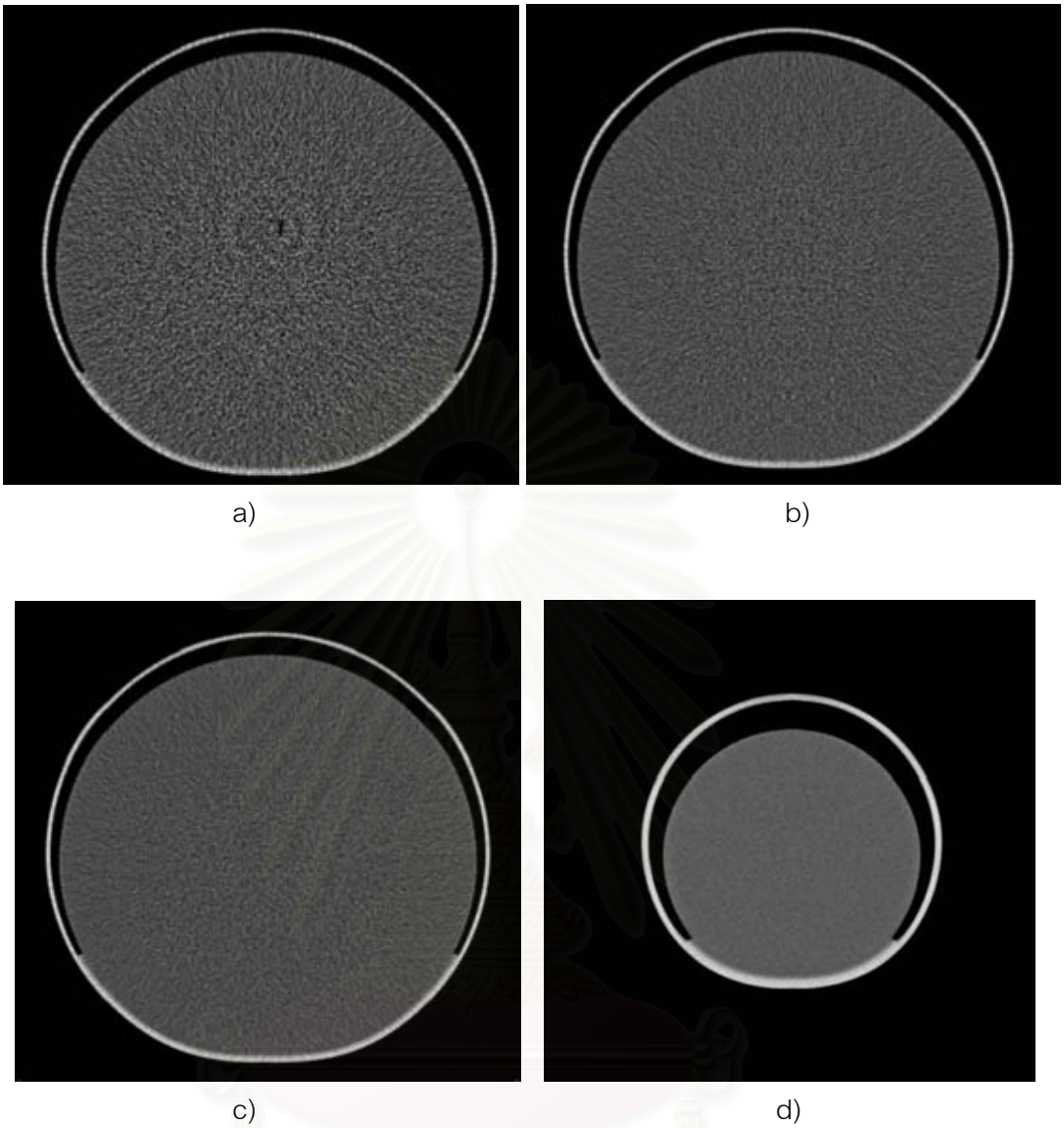

Figure 4.12 The image quality with:
a) score 1- 80 kVp/ 90 mAs_{eff} diameter 25 cm,
b) score 2- 100kVp/ 90 mAs_{eff} diameter 25 cm,
c) score 3- 120kVp/ AEC diameter 25 cm and
d) score 4- 120kVp/ 110 mAs_{eff} at diameter 10 cm.

From results of scoring the image quality by a radiologist. The mean and range of $CTDI_{vol}$ and image noise as shown in table 4.15. The average scores were acceptable and good.

Table 4.15 Score 1-4, number of images and percentage related $CTDI_{vol}$ and noise.

Score	Number of image Total n=60	Percentage (%)	$CTDI_{vol}$(mGy) Mean(range)	Noise (HU) Mean (range)
1	9	15	2.12(1.3-3.02)	27.88(19.18-41.68)
2	25	41.70	3.10(1.17-5.85)	12.02(5.84-20.96)
3	19	31.70	5.15(2.34-8.58)	8.41(4.6-16.36)
4	7	11.70	7.03(5.46-8.58)	4.90(3.46-7.76)

Table 4.16 Score 1-4 related to the number of images from AEC and non AEC systems.

Score	AEC	%	Non AEC	%
1	2	16.7	7	14.5
2	7	58.3	18	37.5
3	3	25.0	16	33.3
4	0	0	7	14.5

In scoring of image quality on AEC and non AEC systems images were the mean and range of $CTDI_{vol}$ and image noise. An AEC, $CTDI_{vol}$ was 2.59(2.16-3.02) mGy and image noise was 23.8(19.18-28.42) HU for not acceptable, 3.22(1.17-5.85) mGy and 10.52(6.88-16.98) HU for acceptable, 6.32(3.35-9.13) mGy and 9.29(5.32-13.08) HU for good and not score of very good. For non AEC system, $CTDI_{vol}$ were 2(1.3-3.02) mGy and image noise were 29.04(23.14-41.68) HU for not acceptable, 3.05(1.3-5.5) mGy and 12.61(5.84-20.96) HU for acceptable, 4.93(2.34-8.58) mGy and 8.25(4.6-16.36) HU for good and 7.03(5.46-8.58) mGy and 4.9(3.46-7.76) HU for very good as detail in table 4.17.

Table 4.17 Score 1-4, related $CTDI_{vol}$ and noise from AEC and non AEC systems.

Score	AEC		non AEC	
	$CTDI_{vol}$ (mGy)	Noise (HU)	$CTDI_{vol}$ (mGy)	Noise (HU)
1	2.59(2.16-3.02)	23.8(19.1828.42)	2(1.3-3.02)	29.04(23.1441.68)
2	3.22(1.17-5.85)	10.52(6.8816.98)	3.05(1.3-5.5)	12.61(5.84-20.96)
3	6.32(3.35-9.13)	9.29(5.32-13.08)	4.93(2.34-8.58)	8.25(4.6-16.36)
4	-	-	7.03(5.46-8.58)	4.90(3.46-7.76)

4.7 Optimal protocol for AEC and non AEC systems.

The characteristics AEC and non AEC systems include results of image noise and $CTDI_{vol}$ to create optimal protocol is shown in table 4.18.

Table 4.18 Optimal protocol for AEC and non AEC systems.

Diameters (cm)	AEC				Non AEC			
	kVp	eff. mAs	$CTDI_{vol}$ (mGy)	Noise (HU)	kVp	eff. mAs	$CTDI_{vol}$ (mGy)	Noise (HU)
10	80	45	1.17	9.36	80	50	1.3	7.84
15	80	59	1.53	12.82	80	70	1.82	11.42
20	100	84	4.2	11.78	100	90	4.5	10.98
25	120	117	9.13	13.08	120	70	5.46	16.58

The optimal protocols appropriate for phantom diameters of 10, 15, 20 and 25 cm are 80, 80, 100 and 120 kVp respectively for AEC mode, the $CTDI_{vol}$ is 1.17, 1.53, 4.2 and 9.13 mGy and image noise is 9.36, 12.82, 11.78 and 13.08 HU. For non AEC mode, the protocol is 80 kVp/50 mAs, 80 kVp/70 mAs, 100 kVp/90 mAs and 120 kVp/ 70 mAs, the $CTDI_{vol}$ is 1.3, 1.82, 4.5 and 5.46 mGy and image noise is 7.84, 11.42, 10.98 and 16.58 HU.

Table 4.19 Paired T-Test of optimal protocol for AEC and non AEC systems.

		Paired Differences					t	df	Sig. (2-tailed)
		Mean	Std. Deviation	Std. Error Mean	95% Confidence Interval of the Difference				
					Lower	Upper			
Pair 1	DOSEAEC - DOSENON	0.737	1.95	0.97	-2.37	3.85	0.75	3	0.506
Pair 2	NOISEAEC - NOISENON	0.055	2.39	1.19	-3.74	3.85	0.05	3	0.966

There is no significantly differences in radiation dose (P = 0.506) and image noise (P= 0.966) between the optimal abdomen protocol for AEC system and non AEC in pediatric with the P-value > 0.05.

CHAPTER V

DISCUSSION AND CONCLUSION

5.1 Discussion

5.1.1 The comparison of CTDI from measurement, displayed and ImPACT values.

The quality control program and verification of radiation dose are important and should be performed prior to the research study. CTDI measurements were compared to the ImPACT scan, the CTDI in air agreed well with the ImPACT value of less than 10% difference. The measurement in phantom showed the difference of greater than 10% because of uncertainty. The $CTDI_{vol}$ displayed on the console when compared to the ImPACT scan the results were accepted of the percent difference of less than 10%.

Uncertainty of CTDI measurement from IAEA TRS 457 [26] are within 6-13% for CTDI in air and 8-14% for CTDI in phantom. The sources of uncertainty include:

- measurement scenario
- precision of reading
- precision of tube loading indicator
- precision of chamber and phantom position
- phantom construction
- chamber respond in phantom

5.1.2 AEC system

AEC systems have recently been implemented to CT units in order to optimize image quality and patient dose. They are designed to adapt the tube current to the patient's shape, size, and the patient attenuation.

The characteristics of AEC implemented in a 16 slice CT scanner were studied with the eff. mAs (tube current modulation) adjusted according to phantom diameters. As the kVp increases, the image noise decreases but increases with the phantom diameters. On the opposite side, the radiation dose increases as the kVp and the phantom diameter increases.

Papadakis AE et al [15] reported that CARE Dose 4D controlled the "image quality reference mAs", adjusted by the user for each clinical protocol. The tube current is adjusted for each rotation, setting a value that is higher or lower than the reference mAs depending upon the size or patient, the attenuation on z axis, relative to Siemens' reference size. The rotational AEC is controlled using feedback from the previous rotation to set the tube current according to the attenuation measured at each tube angle. The AEC system adapts the tube current based on the size and the anatomy of the body region being scanned, relative to a reference patient and the preset image quality reference mAs_{QR} value. For pediatric CT image, the "reference patient" is defined as a 5- year old child with a weight of approximately 20 kg. This

means that in children heavier than 20 kg, the increased attenuation in some body regions, relative to the "reference patient," may imply the increase in the modulated tube current value. Therefore, tube current may potentially exceed the preset mAs_{QR}.

The study demonstrates that tube voltage and tube current influence on radiation dose ($CTDI_{vol}$) on both AEC and non AEC. An AEC system adjusted tube current according to phantom size in order to reduce radiation dose. Non AEC gives the constant $CTDI_{vol}$ according to phantom diameters in each kVp. This results in the problem of poor image quality of large patient. Siegel MJ et al [23] reported the effects of non AEC that the reduced tube voltage cause reduces radiation dose and maintains image contrast. Image noise increases, but the effect is minimal in small phantoms. An additional reduction in tube current further reduces radiation dose.

When selecting technique factors in AEC and non AEC systems, one must also take into account whether there is improvement of image quality. The score of image quality (table 4.15) increases from 1 to 4 as the increasing of the $CTDI_{vol}$ and decreasing image noise. For not acceptable images, AEC and non AEC, depend on low tube voltage 80 kVp for large phantom size (20 and 25 cm). The x-ray photons are not able to penetrate larger phantoms because there is high attenuation coefficient of large phantom. The high kVp of 100 -120 is recommended. The variations of image noise are large because of the low dose.

The image quality from AEC was accepted as 80 kVp at diameter 10 cm, 100 kVp at all phantom size and 120 kVp at 15 cm. Because of the optimization of the dose and the image quality, the maximum acceptable noise is 20 HU as shown in table 4.12. The variations of image noise are less as the increasing dose.

To set the pediatric abdomen CT protocol, after consider the image quality and radiation dose, the appropriate scan techniques according to the phantom diameters was shown in table 4.18. The range of image noise was between 9.36-13.08 HU which are within the acceptable image noise (20 HU) as previous mentioned.

In this study, factors affecting radiation dose are kVp, mAs, phantom diameters and beam energy. The x-ray photons are able to penetrate smaller phantoms diameter because of their less attenuation.

For factors affecting image noise is the CT number. This study, we used agar phantom to determine the noise of CT image, the obtain CT number range from 5-7 HU that this is within acceptable limit (±10HU).

5.1.3 Example of abdomen pediatric patients

A retrospective review of 61 patients in pediatric abdomen CT had been performed at our hospital. As the radiologist prefers non AEC techniques because AEC introduced noise in the image, the data from PACS were mostly non AEC technique. The average and range of $CTDI_w$ for pediatric abdomen in three age groups [27] of 1 year (4 months to 2 years 11 months), 5 years (3 years to 7 years 11 months) and 10 years (8 years to 14 years 11 months) were 2.5(1.50-13.95), 2.82(1.77-13.95) and 10.09(1.99-57.41) mGy, respectively. The $CTDI_w$ reference levels proposed for Europe values are 20, 25 and 30 mGy, respectively [28]. The average and range of DLP were 89.45(47-212), 146.94(50-438) and 528(73-1214) mGy.cm. The DLP reference levels proposed for Europe values were 330, 360 and 800 mGy.cm, respectively. The average and range of effective dose were 2.68(1.14-6.36), 2.94(1-8.76) and 7.92(1.1 - 18.21) mSv, respectively. The AEC technique of 120 kVp and $CTDI_w$ were 7.98(6.84-9.12) mGy.

The average values for $CTDI_w$ and DLP were within the dose reference levels (DRLs), even though the maximum value of DLP were greater than the levels as the dual phase study.

Table 5.1 $CTDI_w$, DLP and E for pediatric abdomen CT scans of 61 patients.

Age groups (years)	No. of patients	Examinations	$CTDI_w$ (mGy)	DLP (mGy cm)	E (mSv)
			Mean (Range)	Mean (Range)	Mean (Range)
1	19	Single phase[a]	2.03 (1.00- 2.99)	78 (38- 158)	2.35 (1.14- 4.74)
	3	Dual phase[b]	3.55 (1.52- 13.95)	160 (100-212)	4.79 (3.00 - 6.36)
5	13	Single phase[a]	2.63 (1.77- 5.69)	128 (50- 438)	2.56 (1.00 - 8.76)
	4	Dual phase[b]	3.03 (1.79- 13.95)	209 (164- 288)	4.18 (3.28- 5.76)
10	17	Single phase[a]	8.71 (2.39- 17.94)	452 (73- 771)	6.79 (1.10 - 11.57)
	5	Dual phase[b]	11.70 (1.99-57.41)	785 (541- 1214)	11.77 (8.12 - 18.21)

[a] represent 1- 2 number of series for abdomen CT examination, such as pre contrast, post contrast.
[b] represent >2 number of series for abdomen CT examination, such as post contrast arterial phase, post contrast venous phase, delay phase, delay kidney, delay bladder.
*[a] and [b] follow radiologist request protocol for the exam depend on clinical or disease.

Table 5.2 The technique factors for 61 patients.

Age groups (years)	kVp	mAs
	Mean	Mean (Range)
1	80	68(25-100)
5	80-100	75(25-110)
10	80-120	103(20-200)

Non AEC technique had been selected, the specific protocols and in the assessment of different clinical indications should be followed for particular scan as in table 5.2.

When compare the data in table 5.2 to our study, it can be concluded that our study agreed with clinical information on pediatric abdomen as in table 5.3.

Table 5.3 Optimal protocol from phantom.

Diameters (cm)	AEC	Non AEC
10	80 kVp	80 kVp/ 50 mAs
15	80 kVp	80 kVp/ 70 mAs
20	100 kVp	100 kVp/ 90 mAs

Therefore, our protocol from phantom study agrees to pediatric study especially abdomen CT.

5.2 Conclusion

In AEC system, the characteristics had been studied which tube current was adjusted according to phantom diameters. The image noise increases to provide for dose reduction. The use of AEC system on CT scan had affected on the dose and noise of the phantom size and technique parameters. For non AEC, the limitation of $CTDI_{vol}$ on the phantom size was observed at the constant $CTDI_{vol}$ at all phantom diameters and different in each kVp. The influence to dose ($CTDI_{vol}$) depends on all parameters of CT that image noise is inversely proportional to the square root of the dose. Therefore, the optimization of radiation dose and image noise is of the high priority.

In order to get the optimization, the protocol for phantom diameters of 10, 15, 20 and 25 cm with related age groups should be 80, 80, 100 and 120 kVp respectively for AEC mode and should be 80 kVp/50 mAs, 80 kVp/70 mAs, 100 kVp/90 mAs and 120 kVp/ 70 mAs for non AEC mode. The pediatric abdomen protocol had been studied and confirmed by the radiologist.

There is no significant difference in radiation dose and image noise between the optimized protocol for AEC and non AEC system ($P>0.05$).

In case of no AEC available in some CT scanners, the determination of optimal protocol must be performed individually to provide the acceptable image noise with the optimal radiation dose.

5.3 Recommendation

In order to use AEC, the pediatric abdomen protocol should be studied for each CT system to optimize the patient dose and reasonable image quality.

McCollough HC et al [14] reported of the AEC systems from each manufacturer are shown in table 5.4 and 5.5, which indicates the capabilities of each system to respond to changes.

Table 5.4 Summary of AEC system capabilities.

Manufacturer	Product name AEC	Z-axis AEC	Rotational AEC
GE	AutomA	AutomA	SmartmA
Philips	DoseRight ACS	-	DoseRight DOM
Siemens	CARE Dose 4D	CARE Dose 4D	CARE Dose 4D/ CARE Dose
Toshiba	SureExposure	SureExposure	-

Table 5.5 Methods for setting AEC image quality level.

Manufacturer	Methods for setting exposure level
GE	'Noise Index' sets required image noise level for the 'Standard' kernel
Philips	System gives same level of image noise as a 'Reference Image' acquired earlier
Siemens	'Reference mAs' is set for standard sized patient
Toshiba	Target image standard deviation is set

REFERENCES

[1] Paterson A and Frush DP. Dose reduction in paediatric MDCT: general principles. Clinical Radiology 62 (2007): 507-517.

[2] Mettler Jr FA, Wiest PW, Locken JA, Kelscy CA. CT scanning: patterns of use and dose. Journal Radiological Protection 20 (2000): 353-359.

[3] Ledenius K, Gustavsson M, Johansson S, Stålhammar F, Söderberg L, Wiklund LM, et al. A method of predicting the image noise in paediatric multi-slice computed tomography images. Radiation Protection Dosimetry 11 (2005): 313-316.

[4] Starck, G., LÖnn, L., Cederblad, A., Forssell Aronsson, E., SjÖstrÖm, L. Alpsten, M. A method to obtain the same levels of CT image noise for patients of various sizes, to minimize radiation dose. British Journal of Radiology 75 (2002): 140-150.

[5] Brooks RA, Chiro GD. Statistical limitations in X-ray reconstructive tomography. Medical Physics 3(4) (1976): 237–240.

[6] Brisse HJ, Ludovic M, Genevieve G, Thomas L, Alexia S, Sylvia N, Bernard A and Jean-CR. Automatic exposure control in multichannel CT with tub current modulation to achieve a constant level of image noise: Experimental assessment on pediatric phantoms. Medical Physics 34(7) (2007): 3018-3033.

[7] Greess H, Nömayr A, Wolf H, Baum U, Lell M, Böwing B, et al. Dose reduction in CT examination of children by an attenuation-based on-line modulation of tube current (CARE Dose). Eur Radiol 12 (2002): 1571–1576.

[8] Greess H, Lutze J, Nomayr A, Wolf H, Hothorn T, Kalender WA, et al. Dose reduction in subsecond multislice spiral CT examination of children by online tube current modulation. Eur Radiol. 14 (2004): 995–999.

[9] Keat N. CT scanner automatic exposure control system. MHRA Evaluation Report 05016 (2005). http://www.impactscan.org

[10] Bushberg J.T, Seibert J. A, Leidholdt Jr E.M, Boone J.M. The essential physics of medical imaging. 2nd ed. USA (2002): 273 –274.

[11] Bronzino J.D. "Computed Tomography" The Biomedical Engineering Handbook 2nd ed (2000).

[12] Nagel HD, Galanski M, Hidajat N, Maier W, Schmidt Th. Radiation Exposure in Computed Tomography. CTB Publications (2002).

[13] " Somatom Sensation 16 Application Guide," Siemens medical.

[14] McCollough CH, Bruesewitz MR, Kofler FM. CT Dose Reduction and Dose Management Tools:Overview of Available Options[1]. RadioGraphics 26(2) (March- April 2006): 503-513.

[15] Papadakis A, Perisinakis K, Damilaks J. Automatic exposure control in pediatric and multidetector CT examinations: A phantom study on dose reduction and image quality. Medical Physics 35(10) (October 2008): 4567-4576.

[16] Kalra MK, Maher MM, Kamath RS, Horiuchi T, Toth TL, Halpern EF, et al. Sixteen-Detector row CT of Abdomen and Pelvis: Study for optimization of Z-axis modulation technique performed in 153 patients[1]. Radiology 233(1) (October 2004): 241-249.

[17] Kalra MK, Maher MM, Toth TL et al. Techniques and Applications of Automatic tube current modulation for CT[1]. Radiology (2004): 233-649.

[18] McNitt-Gray MF. AAPM/RSNA Physics Tutorial for Residents: Topics in CT Radiation Dose in CT[1]. RadioGraphics 22(6) (November-December 2002) : 1541-1553.

[19] Bauhs JA, Vrieze TJ, Primak AN, Bruesewitz MR, McCollough CH. CT Dosimetry: Comparison of Measurement Techniques and Devices[1]. RadioGraphics 28(1) (January-February 2008): 245-253.

[20] Onishi T and Uebayashi SH. Biological Tissue-Equivalent Phantoms Usable in Broadband Frequency range. NTT DoCoMo Technical Journal 7 (4) (March 2006): 61-65.

[21] Srinivasan R, Kumar D and Singh M. Optical tissue-equivalent phantoms for medical imaging. Society for Biomaterials and Artificial organs-India 15 (2) (2002): 42-47.

[22] Cubeddu R, Pifferi A, Taroni P, Torricelli A and Valentini G. A solid tissue phantom for photon migration studies. Physics in Medicine and Biology Issue 10 (October 1997).

[23] Siegel MJ and Schmidt B. Radiation dose and image quality in pediatric CT: Effect of technical factors and phantom size and shape. Radiology 233 (2004): 515-522.

[24] Muramatsu Y, Ikeda S, Osawa K, et al. Performance Evaluation for CT-AEC (Automatic Exposure Control) System. Japanese Journal of Radiological Technology 63(5) (2007): 534-545.

[25] American Association of Physicist in Medicine. Specification and Acceptance testing of Computed Tomography Scanners, Report 39 (May 1993).

[26] International Atomic Energy Agency 2007. Dosimetry in diagnostic radiology: an international code of practice- Vienna: International Atomic Agency (Technical report series, ISSN 0074-1914; no.457). Vienna, Austria: IAEA.

[27] Thomas KE, Wang B. Age-specific effective dose for pediatric MSCT examinations at a large children's hospital using DLP conversion coefficients: a simple estimation method. Pediatr Radiol 38 (2008): 645-656.

[28] Shrimpton PC, Wall B. Reference doses for paediatric computed tomography. Radi Prot 90 (2000): 249-252.

APPENDICES

APPENDIX A

DATA ENTRY FORM

Table I Data entry form at 80 kVp for AEC and non AEC system and eff. mAs at 50, 70, 90 and 110 for non AEC system.

scan AEC of cone phantom				scan Non AEC of cone phantom		
80 kVp			Noise (HU)	80 kVp		Noise (HU)
Diameter (cm)	eff. mAs	$CTDI_{vol}$ (mGy)		eff. mAs	$CTDI_{vol}$ (mGy)	
10				50		
				70		
				90		
				110		
15				50		
				70		
				90		
				110		
20				50		
				70		
				90		
				110		
25				50		
				70		
				90		
				110		

Table II Data entry form at 100 kVp for AEC and non AEC system and eff. mAs at 50, 70, 90 and 110 for non AEC system.

100 kVp				100 kVp		
Diameter (cm)	eff. mAs	$CTDI_{vol}$ (mGy)	Noise (HU)	eff. mAs	$CTDI_{vol}$ (mGy)	Noise (HU)
10				50		
				70		
				90		
				110		
15				50		
				70		
				90		
				110		
20				50		
				70		
				90		
				110		
25				50		
				70		
				90		
				110		

Table III Data entry form at 120 kVp for AEC and non AEC system and eff. mAs at 50, 70, 90 and 110 for non AEC system.

120 kVp				120 kVp		
Diameter (cm)	eff. mAs	$CTDI_{vol}$ (mGy)	Noise (HU)	eff. mAs	$CTDI_{vol}$ (mGy)	Noise (HU)
10				50		
				70		
				90		
				110		
15				50		
				70		
				90		
				110		
20				50		
				70		
				90		
				110		
25				50		
				70		
				90		
				110		

APPENDIX B

REPORT OF COMPUTED TOMOGRAPHY SYSTEM PERFORMANCE

LOCATION: CT room, Chullajakrapong Building
DATE: April 8, 2008
MANUFACTURER: Siemens Sensation 16

Procedure of CT system performance:

1. Scan localization light accuracy
2. Alignment of table to gantry
3. Table increments accuracy
4. Slice increment accuracy
5. Radiation profile
6. Gantry tilt
7. Position dependence and S/N ratio of CT numbers
8. Reproducibility of CT numbers
9. Linearity of CT numbers
10. High contrast resolution
11. Low contrast resolution
12. mAs linearity

1. Scan localization light accuracy

Purpose: To test congruency of scan localization light and scan plane.

Method: Tape localization film to the backing plate making sure that the edges of the film are parallel to the plate edge. Place the film vertically along the midline of the couch aligned with its longitudinal axis. Raise the table to the head position. Turn the alignment light. Mark both internal and external light with unique pin pricks along the midline of the light. Expose the internal light localization using the narrowest slice setting at 120-140 kVp, 50-100 mAs, for external light increment table to light position under software control and expose the film. The center of the irradiation field from the pin pricks should be less than 2 mm.

Results:
Measured deviation = 0 mm
Internal = 0 mm
External = 0 mm

Comment: pass

2. Alignment of table to gantry

Purpose: To ensure that long axis of the table is horizontally aligned with a vertical line passing through the rotational axis of the scanner.

Method: Locate the table midline using a ruler and mark it on a tape affixed to the table. With the gantry untitled, extend the table top into gantry to tape position. Measure the horizontal deviation between the gantry aperture centre and the table midline. The deviation should be within 5 mm.

Table IV Results of alignment of table to gantry.

	Table (mm)	Bore (mm)
Distance from right to centre	202	345
Distance from centre to left	198	355
Measured Deviation	2	5

**Measured deviation = (Distance from right to center - Distance from center to left) / 2*

Comment: Results of alignment of table to gantry were pass.

3. Table increments accuracy

Purpose: To determine accuracy and reproducibility of table longitudinal motion.

Method: Tape a measuring tape at the foot end of the table. Place a paper clip at the center of the tape to function as an indicator. Load the table uniformly with 150 lbs. From the initial position move the table 300, 400 and 500 mm into the gantry under software control (inlet). Record the relative displacement of the pointer on the ruler. Reverse the direction of motion (outlet) and repeat. Repeat the measurements four times. Positional errors should be less than 3 mm at 300 mm position.

Table V Result of table increments accuracy.

Indicated (mm)	Measured (mm)	Deviation (mm)
300	299	1
400	399	1
500	499	1
-300	300	0
-400	400	0
-500	500	0

**Error = | Indicated – Measured |*

Comment: pass

4. Slice increment accuracy

Purpose: To determine the accuracy of the slice increment.

Method: Set up as you would for beam profile measurement. Select 120 kVp, 100 mAs, smallest slit width. Perform several scans with different programmed slice separations under auto control. Scan the film with a densitometer and measure the distance between the peaks.

Table VI Results of slice increment accuracy.

Slice Sep (mm)	Measured Sep (mm)	Deviation
20	20.1	0.1
30	30.2	0.2
50	50	0

**Error = | Slice separation – Measured separation |*

5. Radiation Profile Width

Purpose: To determine the accuracy of pre-patient collimator setting.

Method: Set up as you would for beam profile measurement. Select 120 kVp, 100 mAs , smallest slit width. Perform several scans with different programmed slice separations under auto of control scan. Scan the film with a densitometer and measure the distance between the peaks. Average at least 3 measurements on each profile.

Table VII Results of radiation profile width accuracy.

Collimation (mm)	Measured (mm)	Deviation (mm)
12x0.75 = 9	11.8	2.8
2x5 = 10	10.4	0.4
12x1.5 = 18	20.6	2.6

**Density profiles may also be measured with a scanning microdensitometer or imageJ*

6. Gantry tilt

Purpose: To determine the limit of gantry tilt and the accuracy of tilt angle indicator.

Method: Tape a localization film to the backing plate making sure that the edges of the film are parallel to the edges of the backing plate. Place the film vertically along the midline of the couch aligned with its longitudinal axis. Raise the table to the head position. Move the table into the gantry, center plate to alignment light. Expose the film at inner light location using narrowest slit, 120-140 kVp, 50-100 mAs. Tilt the gantry to one extreme from the console. Record the indicated gantry angle. Expose the film using the above technique. Measure the clearance from the closest point of gantry to midline of the table. Tilt the gantry to its extreme in the opposite direction. Record clearance and repeat the exposure. Measure the tilt angles from the images on the film. Deviation between indicated and measured tilt angles $\leq 3^{o}$. Gantry clearance should be $\geq$30 cm.

Table VIII Results of gantry tilt and gantry clearance.

	Away	Towards
Indicated Angle	15	15
	25	25
Measured Angle	14.9	15.2
	25	25
Deviation	0.1	0.2
Clearance (cm)	38	37

**Error = | Indicated angle – Measured angle |*

Comment: pass

7. Position dependence and S/N ratio of CT numbers

Method: Position the CATPHAN phantom centered in the gantry. Using 1 cm slice thickness, obtain one scan using typical head technique. Select a circular region of interest of approximately 400 mm^2. And record the mean CT number and standard deviation for each of the positions 1 through 5.

Technique: 120 kVp, 250mA, 1s, 300 mm FOV and 10 mm slice thickness

Table IX Results of position dependence and S/N ratio of CT numbers.

Position	Mean CT number	Standard deviation	S/N	C.V.
1 (12 o' clock)	11.1	3.0	3.7	0.270
2 (3 o' clock)	11.1	2.9	3.8	0.261
3 (6 o' clock)	11.5	2.8	4.1	0.243
4 (9 o' clock)	11.3	3.1	3.6	0.274
5 (center)	11.1	3.7	3.0	0.333

**CV = Standard deviation / Mean CT number*

8. Reproducibility of CT numbers

Method: Using the same set up and technique as position dependence, obtain three scans. Using the same ROI as position dependence in location 5, which is the center of the phantom, obtain mean CT numbers for each of the four scans. The coefficient of variation of mean CT numbers of the four scans should be less than 0.002.

Table X Results of reproducibility of CT numbers.

Run Number	1	2	3	4
Mean CT.#	10.279	10.293	10.275	10.307

Mean Global CT. Number	10.2885
Standard Deviation	0.015
Coefficient of variation	0.001

9. Linearity of CT numbers

Method: Set up the CT performance phantom as described in beam alignment. Select the section containing the test objects of different CT numbers. Select the head technique and perform a single transverse scan. Select a region of interest (ROI) of sufficient size to cover the test objects. Place the ROI in the middle of each test object and record the mean CT number.

Technique: 120 kVp, 250 mA, 1 s, 300 mm FOV, and 10 mm slice thickness

Table XI Results of linearity of CT numbers measured by CATPHAN phantom.

Material	Expected CT #	Measured CT #	μ (cm^{-1})
Air	-1000	-1001.9	0
Teflon	990	929.2	0.363
Delrin	340	343.4	0.245
Acrylic	120	123.3	0.215
Polystryline	-35	-38.5	0.171
LDPE	-100	-96.3	0.174
PMP	-200	-186.1	0.227

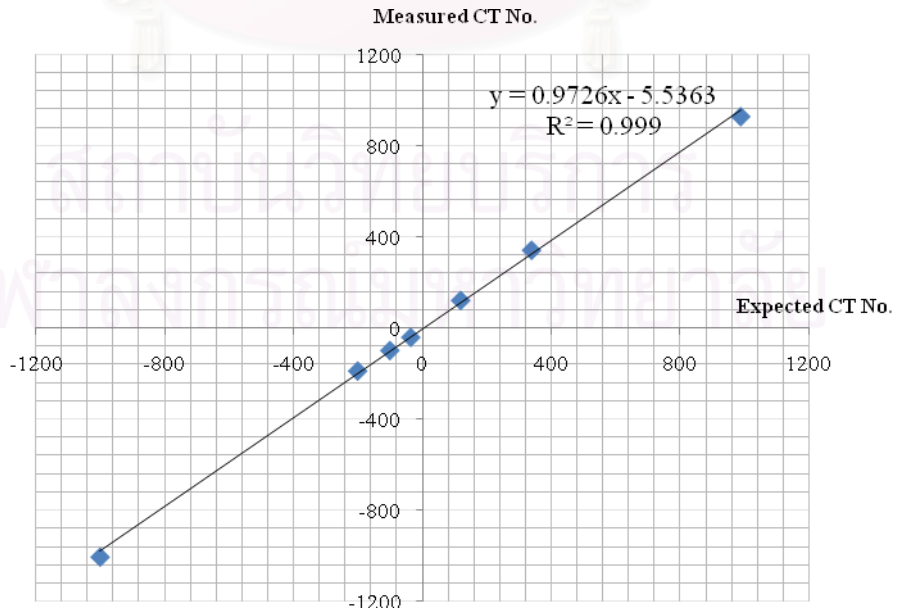

Figure I Linearity of CT number.

10. High contrast resolution

Method: Set up the mini CT performance phantom as described in beam alignment. Select the section containing the high resolution test objects. Select the head technique. Perform a single transverse scan. Select the area containing the high resolution test objects and zoom as necessary. Select appropriate window and level for the best visualization of the test objects. Record the smallest test object visualized on the film.

Technique: 120 kVp, 250 mA, 1 s, 300 mm FOV, and 10 mm slice thickness window width = 150, window level = 200

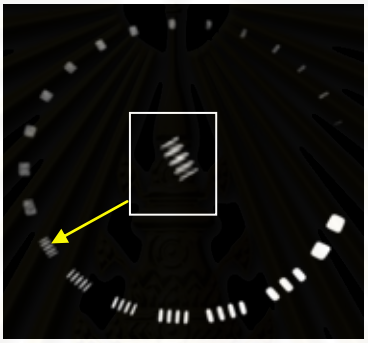

Figure II. High contrast resolution.

Table XII Results of high contrast resolution measured by CATPHAN phantom.

Slice thickness (mm)	Resolution (lp/cm)
10	7 (0.071 cm)

Comment : 7 lp/cm (group visualized)
: 0.071 cm resolution

The 21 line pair/cm gauge has resolution tests for visual evaluation of high resolution ranging from 1 through 21 line pair/cm. The gauge accuracy is ± 0.5 line pair at the 21line pair test and even better at lower line pair tests.

Table XVII Line pair per centimeter high resolution gauge

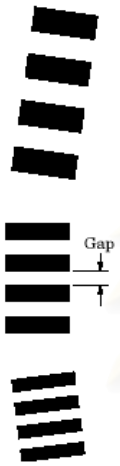

Line pair per cm	Gap size (cm)
1	0.500
2	0.250
3	0.167
4	0.125
5	0.100
6	0.083
7	0.071
8	0.063
9	0.056
10	0.050
11	0.045
12	0.042
13	0.038
14	0.036
15	0.033
16	0.031
17	0.029
18	0.028
19	0.026
20	0.025
21	0.024

11. Low contrast resolution

Method: Select the section containing the low resolution test objects in the mini phantom. Perform a single transverse scan utilizing the same technique as high resolution.

Technique: 120 kVp, 250 mA, 1 s, 300 mm FOV, and 10 mm slice thickness Window width = 140, window level = 100

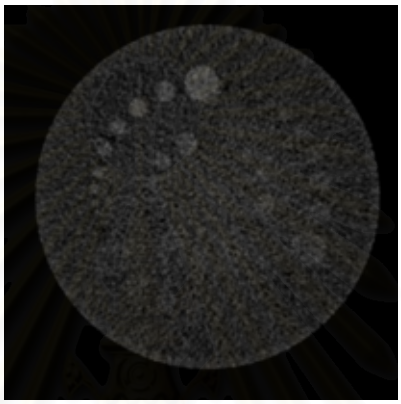

Figure III. Low contrast resolution.

Table XIII Results of low contrast resolution (minimum resolvable diameter [mm]) detected by CATPHAN phantom.

Slice thickness (mm)	Resolution (mm)
10 mm at 1%	2 mm
10 mm at 0.5%	4 mm
10 mm at 0.3%	7 mm

Table XVIII Low contrast module with supra-slice and subslice contrast targets**.**

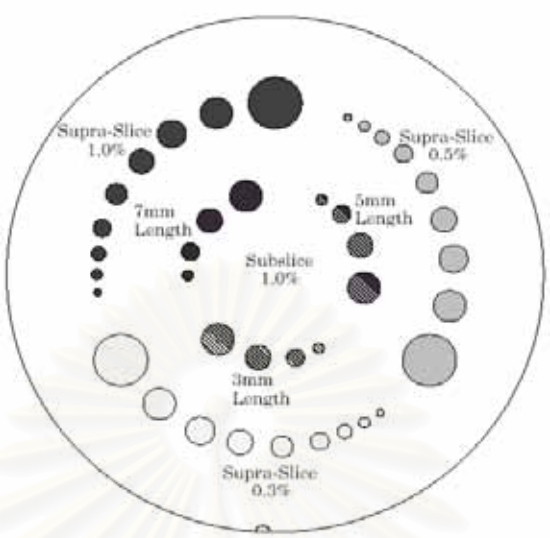

The low contrast targets have the following diameters and contrasts:

Supra-slice target diameters	**Subslice target diameters**
2.0 mm	3.0mm
3.0 mm	5.0mm
4.0 mm	7.0mm
5.0 mm	9.0mm
6.0 mm	
7.0 mm	
8.0 m	
9.0 mm	
15.0 mm	

Nominal target contrast level

0.3 %
0.5 %
1.0 %

12. mAs linearity

Method: Set up the same as position dependence and insert 10 cm long pencil chamber in the center slot of the CT dose head phantom. Select the same kVp and time as used for head scan. Obtain four scans in each of the mA stations normally used in the clinic. For each mA station record the exposure in R for each scan. Scans should be performed in the increasing order of mA. Compute R/mAs for each mA setting.

Technique: 120 kVp, 1 s, 300 mm FOV, and 10 mm slice thickness

Table XIV Results of mAs linearity.

mAs	Exposure in mR				mR/mAs	C.V.
	Run 1	Run 2	Run 3	Run 4		
50	790.7	792.8	793.2	792.2	15.84	1.00
100	1471	1473	1473	1477	14.74	0.036
150	2207	2209	2209	2211	14.73	0.000
200	2948	2951	2954	2950	14.75	0.001
250	3703	3703	3705	3705	14.82	0.002
300	4457	4459	4460	4453	14.86	0.001
350	5221	5224	5224	5228	14.93	0.002

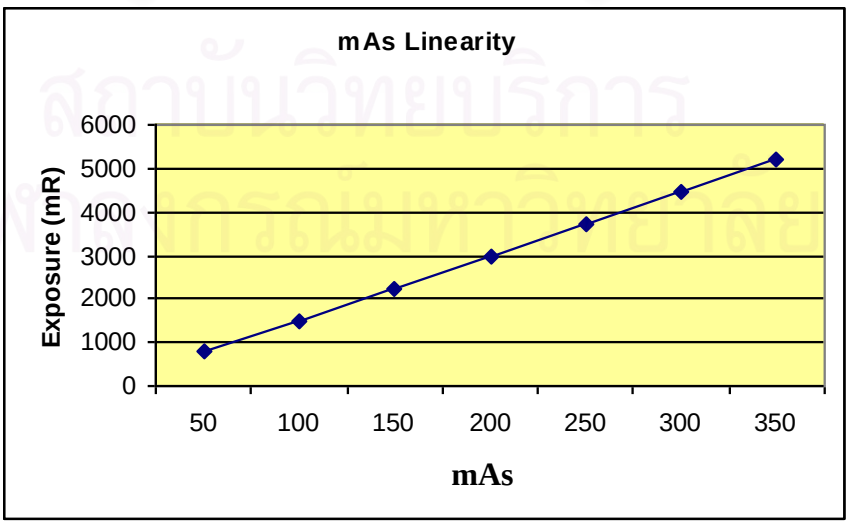

Figure IV Correlation of mR and mAs.

APPENDIX C

SCORING OF IMAGE QUALITY

Table XV Score of image quality**.**

number of image	1=not acceptable	2=acceptable	3=good	4=very good
A1		⁄		
A2		⁄		
A3		⁄		
A4			⁄	
A5			⁄	
B1		⁄		
B2		⁄		
B3		⁄		
B4		⁄		
B5		⁄		
C1	⁄			
C2		⁄		
C3		⁄		
C4	⁄			
C5	⁄			
D1	⁄			
D2	⁄			
D3	⁄			
D4	⁄			
D5	⁄			
E1		⁄		
E2		⁄		
E3			⁄	
E4			⁄	
E5				⁄
F1		⁄		
F2		⁄		
F3			⁄	
F4			⁄	
F5				⁄
G1		⁄		
G2		⁄		
G3		⁄		
G4		⁄		
G5		⁄		

number of image	1=not acceptable	2=acceptable	3=good	4=very good
H1		/		
H2	/			
H3		/		
H4		/		
H5			/	
I1			/	
I2			/	
I3				/
I4				/
I5				/
J1		/		
J2			/	
J3			/	
J4			/	
J5				/
K1			/	
K2			/	
K3			/	
K4			/	
K5				/
L1			/	
L2		/		
L3		/		
L4			/	
L5			/	
60	9	25	19	7
100%	15%	41.70%	31.70%	11.70%

VITAE

NAME	SUPANNEE PASONGCHUN
SEX	Female
NATIONALITY	Thai
DATE OF BIRTH	September 07, 1977.
PLACE OF BIRTH	Roi-Et, Thailand
INSTITUTIONS ATTENDED	Ramkhamhaeng University, 2006: Bachelor of Science (Radiological Technology) Chulalongkorn University, 2009: Master of Science (Medical Imaging)
HOME ADDRESS	61 Moo 6, T. Dokmai, A. Suwannaphu, Roi-Et, Thailand 45130